HANOI UNIVERSITY OF SCIENCE AND TECHNOLOGY

SCHOOL OF ELECTRICAL AND ELECTRONIC ENGINEERING

BACHELOR'S THESIS

Topic:

DIAGNOSIS OF AUTISM SPECTRUM DISORDER USING RESTING-STATE FUNCTIONAL MAGNETIC RESONANCE IMAGING DATA

Student: ĐỖ THỊ MINH PHƯƠNG

KTYS.01 – K64

Supervisor: Dr. NGUYỄN VIỆT DŨNG

Hà Nội, 8-2023

HANOI UNIVERSITY OF SCIENCE AND TECHNOLOGY

SCHOOL OF ELECTRICAL AND ELECTRONIC ENGINEERING

BACHELOR'S THESIS

Topic:

DIAGNOSIS OF AUTISM SPECTRUM DISORDER USING RESTING-STATE FUNCTIONAL MAGNETIC RESONANCE IMAGING DATA

Student: ĐỖ THỊ MINH PHƯƠNG

KTYS.01 – K64

Supervisor: Dr. NGUYỄN VIỆT DŨNG

Dissertation Committee:

Hà Nội, 8-2023

TRƯỜNG ĐẠI HỌC BÁCH KHOA HÀ NỘI
TRƯỜNG ĐIỆN – ĐIỆN TỬ

ĐÁNH GIÁ ĐỒ ÁN TỐT NGHIỆP
(DÀNH CHO CÁN BỘ HƯỚNG DẪN)

Tên đề tài: …….
Họ tên SV: …… MSSV: …….
Cán bộ hướng dẫn: ……

STT	Tiêu chí (Điểm tối đa)	Hướng dẫn đánh giá tiêu chí	Điểm tiêu chí
1	**Thái độ làm việc (2,5 điểm)**	Nghiêm túc, tích cực và chủ động trong quá trình làm ĐATN	
		Hoàn thành đầy đủ và đúng tiến độ các nội dung được GVHD giao	
2	**Kỹ năng viết quyển ĐATN (2 điểm)**	Trình bày đúng mẫu quy định, bố cục các chương logic và hợp lý: Bảng biểu, hình ảnh rõ ràng, có tiêu đề, được đánh số thứ tự và được giải thích hay đề cập đến trong đồ án, có căn lề, dấu cách sau dấu chấm, dấu phẩy, có mở đầu chương và kết luận chương, có liệt kê tài liệu tham khảo và có trích dẫn, v.v.	
		Kỹ năng diễn đạt, phân tích, giải thích, lập luận: Cấu trúc câu rõ ràng, văn phong khoa học, lập luận logic và có cơ sở, thuật ngữ chuyên ngành phù hợp, v.v.	
3	**Nội dung và kết quả đạt được (5 điểm)**	Nêu rõ tính cấp thiết, ý nghĩa khoa học và thực tiễn của đề tài, các vấn đề và các giả thuyết, phạm vi ứng dụng của đề tài. Thực hiện đầy đủ quy trình nghiên cứu: Đặt vấn đề, mục tiêu đề ra, phương pháp nghiên cứu/ giải quyết vấn đề, kết quả đạt được, đánh giá và kết luận.	
		Nội dung và kết quả được trình bày một cách logic và hợp lý, được phân tích và đánh giá thỏa đáng. Biện luận phân tích kết quả mô phỏng/ phần mềm/ thực nghiệm, so sánh kết quả đạt được với kết quả trước đó có liên quan.	
		Chỉ rõ phù hợp giữa kết quả đạt được và mục tiêu ban đầu đề ra đồng thời cung cấp lập luận để đề xuất hướng giải quyết có thể thực hiện trong tương lai. Hàm lượng khoa học/ độ phức tạp cao, có tính mới/tính sáng tạo trong nội dung và kết quả đồ án.	
4	**Điểm thành tích (1 điểm)**	Có bài báo KH được đăng hoặc chấp nhận đăng/ đạt giải SV NCKH giải 3 cấp Trường trở lên/ Các giải thưởng khoa học trong nước, quốc tế từ giải 3 trở lên/ Có đăng ký bằng phát minh sáng chế. **(1 điểm)**	
		Được báo cáo tại hội đồng cấp Trường trong hội nghị SV NCKH nhưng không đạt giải từ giải 3 trở lên/ Đạt giải khuyến khích trong cuộc thi khoa học trong nước, quốc tế/ Kết quả đồ án là sản phẩm ứng dụng có tính hoàn thiện cao, yêu cầu khối lượng thực hiện lớn. **(0,5 điểm)**	
		Điểm tổng các tiêu chí:	
		Điểm hướng dẫn:	

Cán bộ hướng dẫn
(Ký và ghi rõ họ tên)

Điểm từng tiêu chí cho lẻ đến 0,5. Nếu Điểm tổng các tiêu chí > 10 thì Điểm hướng dẫn làm tròn thành 10

ACKNOWLEDGEMENTS

First of all, I would like to convey my most sincere gratitude to my supervisor, Professor Nguyen Viet Dung, for all his patience, guidance and training during this fulfilling journey of four years. Without help from Dr. Dung, I will not be able to finish my research and this thesis. I would like to thank him for always leading the way, supporting me with all my decisions and inspiring me to ask the right questions, which was crucial for the evolution of my thought process and was immensely helpful during the course of my research.

My appreciation goes to all my friends here for their support and advice. My sincere gratitude also goes to all the individuals behind the data, ideas, publications, software, etc. used in my research. Without their contributions, I would not have made this far.

Finally, I wish to thank my great family parents and siblings for their support and encouragement throughout my study.

DECLARATION OF ORIGINALITY

My name is Đỗ Thị Minh Phương – student of class KTYS.01-K64 from School of Electrical and Electronic Engineering. I hereby declare that this submission is my own work and to the best of my knowledge it contains no materials previously published or written by another person, which have been accepted for any other degree or diploma at Hanoi University of Science and Technology or any other educational institution. I also declare that the intellectual content of this thesis is the product of my own work, except to the extent that assistance from others in the project's conception, presentation and linguistic expression is acknowledged.

Hanoi, August 4th, 2023

Supervisor	**Student**
Dr. Nguyễn Việt Dũng	**Đỗ Thị Minh Phương**

TABLE OF CONTENT

LIST OF ABBREVIATIONS

AAL	Automated Anatomical Labelling
ABIDE	Autism Brain Imaging Data Exchange
ADHD	Attention-Deficit Hyperactivity Disorder
ANN	Artificial Neural Network
ASD	Autism Spectrum Disorder
AUC	Area Under The Curve
BOLD	Blood-Oxygen-Level-Dependent
CAD	Receiver Operating Characteristics
CDC	Computer-Aided Diagnosis
CT	Centers for Disease Control and Prevention
DWI	Diffusion-Weighted Imaging
EEG	Electroencephalographic
FC	Functional Connectivity
FFNN	Feed-Forward Neural Networks
fMRI	Functional Magnetic Resonance Imaging
H-O	Harvard-Oxford
LSTM	Long Short-Term Memory
MEG	Magnetoencephalography
ML	Machine Learning
MNI	Montreal Neurological Institute
MRI	Magnetic Resonance Imaging
MRS	Obsessive-Compulsive Disorder
OCD	Oppositional Defiant Disorder
ODD	Oppositional Defiant Disorder
RNN	Recurrent Neural Network
ROC	Receiver Operating Characteristic

ROI	Region-Of-Interest
rs-fMRI	Resting-State Functional Magnetic Resonance Imaging
SOM	Self-Organizing Map
SVC	Support Vector Classifier
SVM	Support Vector Machine
TC	Typical Control

LIST OF FIGURES

LIST OF TABLES

ABSTRACT

Autism Spectrum Disorder (ASD) is a largely prevalent neurodevelopmental condition with a big social and economical impact affecting the entire life of families. It refers to a wide range of behavioral and social abnormality and causes problems with social skills, repetitive behaviors, speech, and nonverbal communication. Even though there is no exact cure to ASD, an early diagnosis can help the patient take precautionary steps. Diagnosis of ASD has been of great interest recently, as researchers are yet to find a specific biomarker to detect the disease successfully. For the diagnosis of ASD, subjects need to go through behavioral observation and interview, which are time-consuming and not accurate sometimes . Also, there is a lack of dissimilarity between neuroimages of ASD subjects and typical control (TC) subjects which make the use of neuroimages difficult for the diagnosis. So, computer aided diagnosis (CAD) approaches using machine learning and deep learning to diagnose ASD are becoming popular day by day. In the CAD-based approach, features are extracted either from the functional MRI images or the structural MRI images to build the models.

In this thesis, I presented machine learning – based and deep learning – based approaches to detect peoples with ASD from healthy people. This thesis carried out a comprehensive exploration of the impact of the choices involved while building these machine learning and deep learning pipelines. The pipeline of this thesis encompassed the estimation of the functional connectivity matrix from brain parcellations or brain atlases, feature extraction and building classification models for ASD prediction. allowing to detect people with ASD from normal people. At first, BOLD time-series signals were extracted and brain connectivity networks were created from the resting-state functional MRI (rs-fMRI) images by using the region-of-interest (ROIs)-based parcellation scheme. Next, machine learning-based approaches using several classical machine learning classifiers such as support vector machines, logistic regression, and ridge, etc. were ultilized for ASD and TC classification of all combinations of three brain atlases including Automated Anatomical Labelling (AAL), Harvard-Oxford (H-O) and Juelich. Using the proposed method on Autism Brain Imaging Data Exchange

(ABIDE) and optimizing training parameters using 10-fold cross-validation, the best result was obtained using Juelich atlas and non-parse support vector machine classifier with an accuracy equal to 69.00%. Besides, a deep learning model using Long Short-Term Memory (LSTM) network was built for ASD classification and feature selection. The classification accuracy of the LSTM classifier based on test dataset is 78.24%. Results of this thesis demonstrate that the meaningful brain biomarkers of ASD can be extracted by applying machine learning and deep learning techniques on brain rs-fMRI data. This data-driven technique can be a powerful tool for early detection and understanding brain anatomical underpinnings of ASD.

Keyword: machine learning, deep learning, rs-fMRI, functional connectivity, autism spectrum disorder (ASD), classification, ABIDE

CHAPTER 1. INTRODUCTION

This chapter presents the background and motivation for this thesis in section 1.1. Section 1.2 describes the objectives of this research work. A summary of the generated contributions is given in section 1.3. Section 1.4 presents the organization and structure of this thesis.

1.1. Background and Motivation

Autism Spectrum Disorder (ASD) [1] is a highly prevalent, heritable and heterogeneous neurodevelopmental disorder that has distinctive cognitive features often cooccuring with other psychiatric or neurological disorders. The Center of Disease Control and Prevention (CDC) has reported the number of patients with ASD to have increased by 30 percent with the number of subjects diagnosed jumping from one in 88 children to one in 59 children over the period of ten years. In today's world where technology has advanced by leaps and bounds, there is still no accurate test for ASD. In case of disorders like ASD, the earlier it is diagnosed, higher are the chances of effectively helping the subject by reducing the symptoms. The symptoms of ASD can sometimes be observed as early as 18 months of age or earlier [2]. However, most of the subjects do not receive their final diagnosis till they are much older. The only proven method to diagnose ASD is by observing the subject over a period and analyzing their behavior and development. The traditional diagnosis process includes Autism Diagnostic Observation Schedule [3] and Autism Diagnostic Interview [4]. But, these diagnosis processes are time-consuming and can be at fault sometimes, as there are no specific behaviors that can be described as ASD. So, it is necessary to invent ways that can diagnose ASD more accurately and more efficiently without relying on the behavioral pattern.

Recently, using machine learning algorithms for the diagnosis of ASD has become popular. It is necessary to define features to train a machine learning classifier. The features need to be discriminative, for the classifiers to work efficiently. There are different ways to determine the features. The structural property of the brain can be

used as features where the property of different regions are studied and if there is any change due to a particular disease the change is used as a feature [5]. The phenotypic information of the patients [6] and the behavioral attributes [7] can also be incorporated into the study and used as features. However, the features used in the mentioned studies to diagnose ASD aren't discriminative and competent enough as they lack having a satisfactory classification result over a larger dataset. Taking inspiration and motivation from such findings and drawbacks above, in this thesis, I have proposed a framework for detection of ASD using features extracted from rs-fMRI data.

1.2. Thesis Objectives

The main objective of this thesis is to investigate the effectiveness of machine learning approaches, including newer deep learning techniques, for computer-aided diagnosis (CAD) of individuals with autism spectrum disorder (ASD) compared to typically control (TC) children.

The focus will be on classification, with the aim of distinguishing between those with ASD and those who are healthy controls. The study will also examine the impact of various metaparameter choices such as brain parcellations and classifiers in the computational pipeline, with the ultimate aim of identifying the optimal combination of these choices.

1.3. Thesis Contributions

In summary, our contributions in this study are as follows:

(1) Showing potential of using machine learning and deep learning algorithms applied to rs-fMRI for automatic detection of ASD.

(2) Implement the combination of three brain atlases, six machine learning classifier algorithms with cross validation procedures and LSTM-based classification model in ASD detection and having performance result collection and analysis.

(3) Identify top correlated brain regions of ASD and TC subjects as potential biomarkers that should be more deeply investigated in future works.
(4) Highlight future directions to improve the performance of such frameworks for automatic detection of ASD.

1.4. Thesis Organization

This thesis is structured as follows:

Chapter 1 presents the background and motivation of this thesis. This chapter also formulates the problem that this thesis trying to solve and mentioned the objectives needed to be achieved.

Chapter 2 provides a detailed theoretical background on ASD, rs-fMRI, as well as the description of diagnostic methods that are applied in the search of optimal detection of ASD subjects.

Chapter 3 discusses the methodology framework used in this thesis.

Chapter 4 reports the results achieved with machine learning and deep learning techniques over the ABIDE database. In this chapter, the results of feature extraction results and top correlated brain regions of ASD and TC subjects are also presented.

Chapter 5 concludes remarks about this thesis presented along with the indication of possible future directions.

CHAPTER 2. THEORETICAL BACKGROUND

In this chapter, I review the theoretical background used in this thesis for the diagnosis of autism. The contents of the chapter are as follows: Section 2.1 presents the brief information about ASD. Section 2.2 presents the ASD diagnostic methods and some recent studies on diagnosis of ASD. Section 2.3 defines the brief background on neuroimaging which is resting-state functional imaging in particular.

2.1. Autism Spectrum Disorder (ASD)

Autism spectrum disorder (also known as ASD) is a range of lifelong developmental neurobehavioral disorders. It refers to a broad range of conditions characterized by impaired social skills, co-occurring behaviors, reduced speech, and nonverbal communication, depression, anxiety, attention deficit, and a limited extent of interests and activities that are carried out differently and begins since early childhood. It is prevalent and heterogeneous with an estimated average of 1% of global population [8] and 1 in 66 children in Canada which included 1 in 42 boys and 1 in 189 girls according to the report of the 2018 national autism spectrum disorder surveillance system (NASS) [9]. The Center of Disease Control and Prevention (CDC) has recorded the number of subjects diagnosed with ASD to have increased by 30 percent with the number of subjects diagnosed jumping from one in 88 children to one in 59 children over the period of ten years [10]. The percentage has the trend to increase in the past decades [11]. In Vietnam, there is currently no official research data available on the exact number of children with ASD. However, according to statistics released by the General Statistics Office of Vietnam in January 2019, there are approximately 6.2 million people with disabilities aged 2 years and above, out of which around 1 million are estimated to have ASD. The prevalence rate of children with ASD is estimated to be around 1% of all children born.

The term '*spectrum*' in ASD indicates the wide range of symptoms and severity possessed by ASD patients. The disorders of ASD include difficulty with communication and interaction with other people, restricted interests and repetitive

behaviors and symptoms that hurt the person's ability to function properly in school, work, and other areas of life [12]. The earliest reports of the ASD phenotype are attributed to Kanner [13] and Asperger [14]. In these foundational works Kanner and Asperger both detail case studies of children in which typical autistic behaviors are observed. By definition ASD is phenotypically heterogeneous, encapsulating a spectrum of individuals whose behavioral deficits range from severe impairment (e.g. learning disability, non-verbal) to high functioning (e.g. average or above average IQ, relatively minor impairments to social communication) [15]. In addition to the core features, individuals with ASD experience high rates of comorbidity with other psychiatric and medical conditions including; social anxiety disorder, attentiondeficit disorder (ADD), attention-deficit hyperactivity disorder (ADHD), oppositional defiant disorder (ODD), obsessive-compulsive disorder (OCD), specific phobia, gastrointestinal problems, and epilepsy [16] (Figure 2.1).

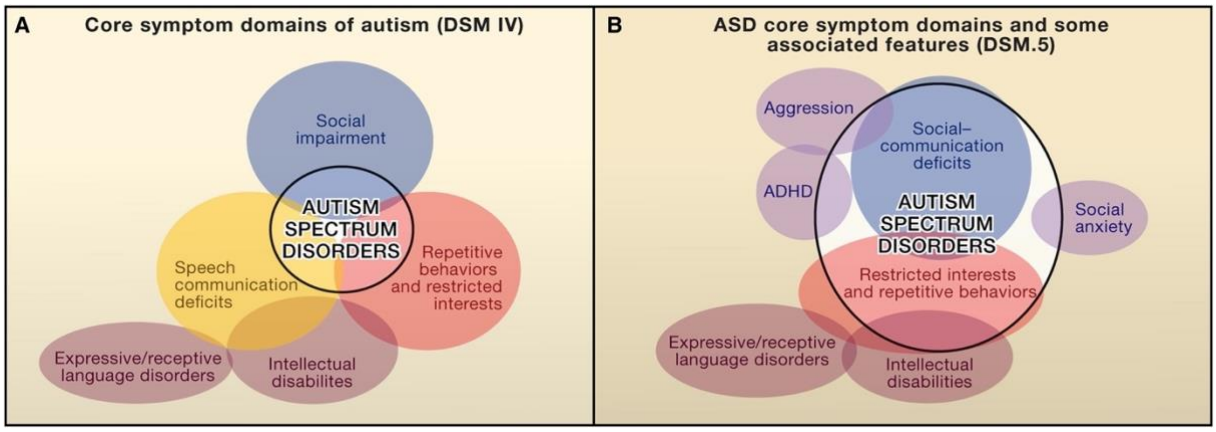

Figure 2.1 The Autism Spectrum

ASD is a developmental disorder which refers to symptoms generally appear in the first two years of life. As developmental diseases are heterogeneous and lifelong disorders, treatments and services can improve a person's symptom and ability to function. Early detection of ASD is effective in decreasing impairments for children and helping improve the quality of life for ASD patients. At the same time, it can alleviate the economic cost for both the society and patient families. Moreover, lack of time and training can deter pediatric screening. The American academy of pediatrics recommends that all children be screened for autism [17]. The modified checklist for autism in toddlers revised (M-CHAT-R) is a widely used screener but requires follow-up questions and error-prone human scoring and interpretation. Besides, the

uncertainty associated with the symptoms and neurobiological properties make autism screening challenges. Furthermore, these uncertainties lead to great heterogeneity in the subjects and are the reason for the spectrum of diseases [18].

ASD is a complex and highly heterogeneous disorder, involving whole-brain structures and functions, which makes the diagnosis very challenging. Currently, ASD diagnosis is typically based on clinical interviews and observation of the individual's behavior and intellectual abilities. This kind of diagnosis procedure can be subjective, time consuming and unreliable because the behavioral symptoms related with ASD is difficult to be observed from a child. Diagnosing ASD requires long-term behavioral observations by a specialist and often costing thousands of dollars. Therefore, besides the challenges of diagnosis of ASD faced by patients and their families, the economic cost of ASD is very high. A recent study [19] estimated that ASD's economic cost of 2015 was $268 billion in the United States. The study projects annual costs will rise to $461 billion in 2025 and more than $1 trillion by 2025 if ASD's prevalence remains constant and keeps the rising rate as before. In summary, tremendous effort is needed for medical assessment to find effective ways to diagnose ASD and alleviate the burden of patient families and the society.

2.2. Diagnosis of Autism Spectrum Disorder

2.2.1. Traditional Methods

ASD is currently diagnosed on the basis of qualitative information obtained from parent interviews and clinical observation, which leads to disturbing differences between sites. Given its great prevalence, automated approaches to assist diagnosis [20] are highly desirable. Increasingly, clinical neuroscience focus is shifting to find metrics derived from brain imaging [21] that may be useful to predict diagnostic category, disease progression, or response to intervention, e.g. looking for endophenotype using multivariate analysis approaches [22]. These metrics come from machine learning approaches to the study of brain structure and function. Some of them can be considered as neuroimage based biomarkers that would be helpful to guide early interventions. Currently, the research community has not yet identified reliable and reproducible biomarkers for ASD. Clinical heterogeneity, methodological

standardization and cross-site validation raise issues that must be addressed before further progress can be achieved [23].

2.2.2. Recent Researches on ASD Diagnostic Method

2.2.2.1 Introduction on computer-aided diagnosis (CAD)

Computer-aided diagnosis (CAD) aims to help the clinical practitioner to achieve early and accurate diagnosis of ASC in order to try to apply early treatments hoping to improve the child's condition in some way. Recent randomised control trials [24] emphasize the improved effect achieved when the treatment is applied at early ages, even todlers. Here this thesis will not discuss the clinical aspects such as treatment protocols or diagnositic procedures follow in the clinic, focusing only on the technological aspects. A CAD system often is composed of some technological device that allows to measure the behavior or some biological or physiological aspect of the subject, and some classifier system built by machine learning techniques that provides the diagnosis suggestion. Machine learning can be used to build hierarchies of categories which may help to refine diagnostic process [25], but mostly is used to give a response to the question "Is this child at high risk of ASD?". It is important to keep in mind that ASD is a quite heterogeneous condition that is still under revision by the clinical experts, therefore all the technological solutions would be always limited in their scope by some a priori selection of measures and expected observations.

2.2.2.2 Behavioral-based CAD methods

There are various approaches to detect autism that involve measuring behavioral information through computer vision or other sensing techniques. Some of these approaches are based on an enactive approach to autism understanding [26], which focuses on disruptions to action perception [27]. Other approaches involve measuring a child's response to stylized representations, such as discriminating between geometric figures [28]. A wide variety of sensors can be used to monitor behavior and assess the risk of autism, either on their own or in combination with other sensors. For example, one study proposed using computer vision to measure the imitation response of children with autism spectrum disorder (ASD) compared to neurotypical children [29]. Another study used the inertial information of a smart tablet to detect patterns of

motion that are compatible with ASD clinical characterization, such as larger and faster motions and stronger forces at contact [30]. Another approach used the Kinect V2 sensor to measure the motions of subjects and detect stereotypical motor reactions, which are a hallmark of autism in clinical diagnosis processes. Experiments using motion captured from professional actors showed that this detection can be achieved with great probability [31]. A study reported achieving discrimination of children at high risk versus low risk of ASD by detecting motion through wrist accelerometers during certain motor tasks [32]. Similarly, tracking body motion while engaging with a social robot was found discriminant in [33]. Computing the dynamic time warping (DTW) distance between the robot motion and the child motion while engaging in an imitation game was intended as a measure of impairment in [34]. The examination of the gaze and the pupil while interacting with a robotic avatar has been also shown to be lead to moderate classification accuracy [35]. The measurement of eye motion when tracking objects by means of an electrooculogram has been also show capable of high accuracy discrimination of ASC subjects [36], while serving also to train the subjects to perform more accurate object tracking. The responses to a mismatch experiment of sounds including vowel, vowel duration, consonant, syllable frequency, syllable intensity showed significant differences in children (8-12 year old) with asperger syndrome in intensity and frequency relative to typically developing children [37] leading to conclude aberrant cortical sound-speech discrimination in Asperger syndrome children. Conversation analysis is used while a ASC child is interacting with a robot trying to ascertain if he has perseverative talking features [38] one of the traits of high performing ASD children. The sequential analysis showed that recurrence may be driven by the interaction scenario. Other experiments measured the response of ASD versus TC children when viewing silouhettes of human and robotic [39] measuring the mimicry as the project results.

2.2.2.3 EEG-based CAD biomarkers methods

Researchers have used electroencephalographic (EEG) sensors to explore the possibility of identifying brain biomarkers of autism spectrum disorder (ASD) or implementing computer-aided diagnosis (CAD) systems based on EEG readings. Some studies have successfully distinguished between ASD and typically developing (TD) children in small groups using feature extraction techniques that include non-

linear chaotic time series analysis and time-frequency decomposition, such as fractal dimension [40]. Another proposed computational pipeline involves wavelet decomposition, entropy feature extraction from each EEG sub-band, and a classifier based on artificial neural networks (ANNs) [41]. Another type of ANN uses self-organizing maps (SOM) for feature extraction and reports results of a number of conventional classifiers upon the SOM features [42]. However, classification-oriented research does not provide clinical or biological insights because it is often impossible to translate significant features back into biological causes or biomarkers that can be useful for understanding the condition and proposing treatments. In search of biomarkers, a recent systematic review of studies that used EEG and magnetoencephalography (MEG) data for brain connectivity analysis reports underconnectivity in long-range connections for ASD subjects, while local connections seem to be unaffected. Recent approaches have combined EEG information with other sources such as MRI information [43].

2.2.2.4 MRI-based CAD biomarkers methods

Researchers have used various types of magnetic resonance imaging (MRI) to investigate whether there are any anomalies in brain morphology and functional connectivity that could serve as biomarkers for autism spectrum disorder (ASD). The most relevant MRI modalities used in the literature for this purpose are structural MRI, resting-state functional MRI (rs-fMRI), diffusion-weighted imaging (DWI), and magnetic resonance spectroscopy (MRS) [44]. The goal of biomarker identification is to find brain regions, connections, or biochemical signatures that show significant differences between individuals with ASD and those who are neurotypical. Image biomarker findings are quite diverse. Structural MRI findings using voxel-based differences are sometimes contradictory and inconsistent, and heavily dependent on the technique used and the age of subjects, though some increase in gray matter and white matter volume was consistently reported, as well as corpus callosum decrease in volume. Morphological differences in thalamus and striatum have been also reported using structural features [45]. Tractography analysis based on fractional anisotropy coefficients extracted from DWI data have shown consistent degradation of main neural tracts, pointing to a degradation of brain connectivity. The study of brain connectivity in toddlers comparing ASC with other developmental disorders has been

reported using DWI and streamlined tractography [46]. Over an anatomical parcellation of the brain, the neural path-ways between them were extracted, and the connectivity strength between brain regions was estimated. The results point to overconnectivity in ASC toddlers versus other developmental disorders.

Computer-aided diagnosis (CAD) takes brain biomarkers identification a step further by producing a decision on the diagnosis that can be used by clinical practitioners with some confidence. However, CAD systems require sophisticated machine learning tools, such as multiview multitask ensembles of classifiers [47]. In one study, a multimodal approach was used that involved both structural and functional MRI. Nonstationary independent components were extracted as fMRI features, and a sparse autoencoder was used to extract texture features from the structural MRI. These features were then used to train and test a support vector machine (SVM) classifier, which was able to classify children into those with autism spectrum disorder (ASD) and those without [48]. Another study used decision tree classification on features extracted from multimodal MRI data, although the sample size was very small [49]. In yet another study, random forest classifiers were used and achieved much better classification accuracy than SVM with recursive feature extraction [50]. Deep learning is also having a significant impact on recent attempts to construct computer-aided diagnosis (CAD) systems. For example, Deep Belief Networks have been reported to successfully discriminate between children with ASD and those without by fusing structural and functional MRI data [51]. Another approach used sparse autoencoders to extract feature filters from structural MRI, which were then applied to 3D structural MRI data using a convolutional neural network for feature extraction [52]. A tensor based approach to estimate connectivity in rs-fMRI is proposed in [53] that it is able to extract both the connectome representation and the dynamic functional connectivity for each subject finding discriminant effects on the putamen connectivity for ASC subjects. Fine temporal analysis of the rs-fMRI time series, by clustering them into short time intervals that may be shared between brain regions, allows more precise classification [54]. On the other hand, structural features of brain cortex were used by random forest classifier to produce reliable predictions in toddlers [55].

2.3. Resting-state Functional Magnetic Resonance Imaging (rs-fMRI)

2.3.1. Neuro-imaging

Neuro-imaging sciences endeavor to measure brain activity from human or animal subjects and relate it to experimental conditions and behavior observations. It is founded on the observation that cognition has measurable effects on the brain, that are somehow shared across subjects, and to some extent across species. Brain imaging includes the use of diverse techniques to image the structure, function, and biochemical processes of the brain. Imaging technologies of various modalities now provide the visualization of the structure and function of the brain with high resolution. Neuro-imaging is becoming an important technique in both research and clinical care. It is being successfully used to facilitate the understanding of the structure and the functions of the brain and also has been a vital diagnostic tool for many neurological disorders [56]. Neuro-imaging can be broadly categorized into three categories: structural, functional, and molecular imaging [57].

Structural imaging techniques are used to capture the physical structure of the brain and include X-ray, Computer Assisted Tomography (CT), MRI, Diffusion Tensor Imaging (DTI), and others. MRI uses radiofrequency waves to examine tissue structure based on the principle of nuclear magnetic resonance. DTI is a specific type of MRI that measures the diffusion of water in tissues to characterize microstructural changes [58]. DTI is commonly used to estimate white matter connectivity patterns in neurological disorders such as autism spectrum disorder (ASD) and attention-deficit/hyperactivity disorder (ADHD).

Functional imaging techniques are used to capture brain function, physiology, or metabolism [59]. Techniques such as functional Magnetic Resonance Imaging (fMRI) and Positron Emission Tomography (PET) measure cerebral blood flow as an indicator of brain metabolism, assuming that active brain regions have higher blood flow.

Molecular and cellular imaging techniques are used to examine the biochemical activities of cells and molecules [60]. These techniques typically use light microscopes and light-emitting probes that emit radio frequencies of various wavelengths to contrast the target cells.

In addition to unimodal studies that focus on a single imaging modality, there are also studies that combine information from multiple imaging modalities to gain a more comprehensive understanding of brain structure and function [61].

This thesis makes an effort to identify brain markers for ASD detection using the brain images captured by fMRI. So, this thesis will limit our scope to fMRI from here on.

2.3.2. Magnetic Resonance Imaging (MRI)

MRI is a non-invasive tool for examining the anatomy of the human body. It is based on the principle of magnetic resonance imaging and it utilizes the magnetic properties of the proton of the hydrogen atom which is abundant in our body. A typical MRI machine consists of three major components: a very strong main magnet, gradient magnets, and a radio frequency emitter. A typical MRI process includes four major components: slice selection, phase encoding, frequency encoding, and signal reconstruction (Figure 2.2) [62].

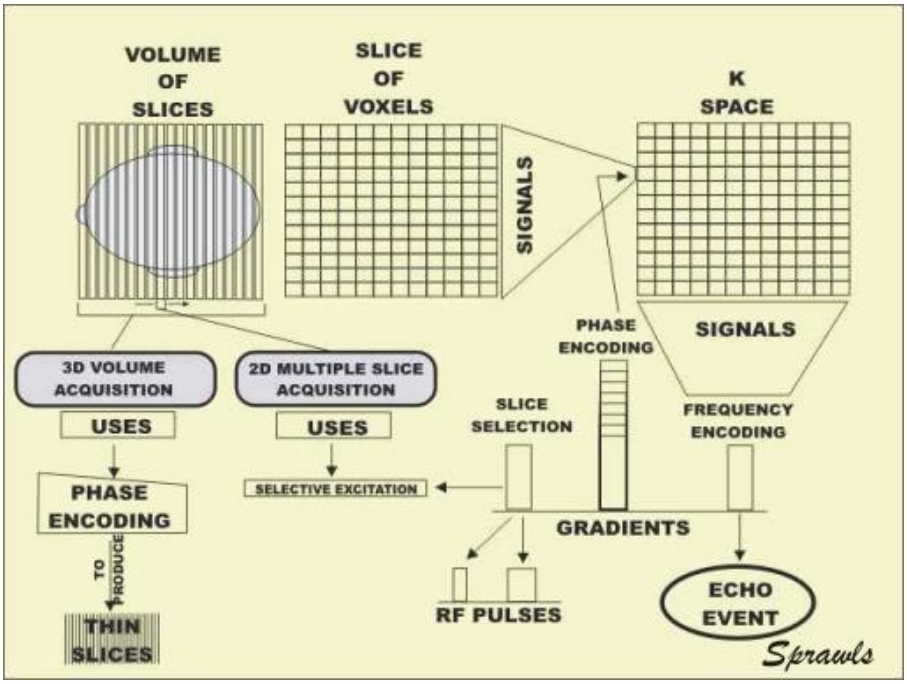

Figure 2.2 MRI acquisition process

Slice selection: Protons in the body can act like small magnetic dipoles, spinning around their axes. Initially, these dipoles are randomly aligned. However, when a strong external magnetic field is applied in an MRI machine, the dipoles start to

precess along the direction of the external field at a frequency called the Larmor frequency, which is proportional to the strength of the external magnetic field. To create an image, a combination of gradient magnets is turned on, which causes the net magnetic field to vary linearly along the axis perpendicular to the 2D slice of interest. This means that the protons in each slice are precessing at a unique frequency and can only absorb electromagnetic waves of particular frequencies to resonate, echo, or excite. In other words, by varying the net magnetic field, we can selectively excite only the hydrogen atoms in the slice of interest. This allows us to create an image of that specific slice, while ignoring other slices.

Phase encoding: During phase encoding in an MRI scan, a radio frequency pulse is used to excite only the hydrogen atoms in the slice of interest. Once the pulse is turned off, these atoms gradually return to a low energy state and emit electromagnetic waves at their precessing frequency. Another set of gradient magnets is then turned on, which causes the net magnetic field along one axis of the slice of interest to vary. This variation results in protons at different locations precessing with different frequencies and creating a location-dependent phase lag relative to their initial state. This phase lag effectively encodes the spatial information in the slice of interest. To ensure that enough information is captured to reconstruct the anatomical image, several phase encoding steps are repeated.

Frequency encoding: After phase encoding, another gradient is applied along the axis perpendicular to the phase encoding axis. This gradient causes the hydrogen atoms at different columns to precess with different frequencies proportional to the net magnetic field. This process is called frequency encoding and helps to further encode spatial information in the image.

Signal reconstruction: The excited hydrogen atoms return to a low energy state and release electromagnetic waves. These waves have a frequency and phase that depend on their spatial location, and are picked up by receiver coils to create a 2D signal called k-space. A Fourier Transform is then applied to the k-space image to reconstruct the 2D anatomical image of the slice. Multiple 2D slices are collected and combined to form the 3D MRI volume.

2.3.3. Functional Magnetic Resonance Imaging (fMRI)

This thesis focuses on fMRI, a modality introduced by Ogawa et al. (1990) [63]. This mean of observation, which is performed in an MRI scanner, is non intrusive yet it provides a satisfying temporal and spatial resolution. Unlike Electro-encephalography (EEG) and Magneto-encephalography (MEG), functional MRI does not directly measure electric of magnetic field that are stemmed by neurons in activity. In contrast, it leverages Magnetic Resonance Imaging [64] to measure the variation in the level of oxygenated and deoxygenated blood within the blood vessels that irrigate neurons. As spiking neurons require hemoglobin-provided dioxygen to produce energy, a neuronal activity increase in any volume of the brain is followed within five second by an increase of oxygenated blood in this volume and by an undershoot that lasts roughly 30 seconds. These oxygen-dependent variations are detectable through Magnetic resonance imaging (MRI), and are extracted as the Blood-oxygen-level dependant (BOLD) signal.

Modelisation: The biological phenomena at stake are modelled as such: the observed BOLD signal is the result of convoluting the neuronal activity in the volume of interest with an Hemodynamic-response function (HRF), that models delay, amplitude and under-shoot of the level of oxygenated blood within this volume. At the end of the fMRI acquisition, we obtain a sequence of brain images, i. e. one time-series per voxel that records the intensity of the neural activity, convoluted by the hemodynamic response, within this voxel, plus noise from various sources. Typically, these time-series have a period of 0.8 to 3 seconds, and the space resolution (i. e. the volume of each voxel) varies from 1 mm^3 to 27 mm^3, depending on the spatial resolution that the scanner allows. Note that these volumes contain millions of neurons: although functional MRI has a good spatial resolution compared to other non intrusive modalities, it is still many orders of magnitude above the cellular level.

Preprocessing: fMRI raw data must typically be corrected for various noise sources that deteriorate the signal-to-noise ratio of the BOLD time series. Most importantly, subject head motion is recorded and regressed through within-record registration, as are physiological conditions (heart-beat, respiration). The physical artifacts related to the scanning process (e. g., the fact that slices are recorded one after another, causing time jitter, and the non-uniformity of the base magnetic field) are also

monitored and compensated in preprocessing steps. Typically, the public datasets on which the thesis developed new techniques are already provided as pre-processed time series for which physiological and physical confounds have already been regressed.

Group-level analysis: In most functional MRI studies, the same acquisition protocol is performed on different subjects and potentially several times on each subject. Analysis of the BOLD signal may then be performed at a subject-level, or at the group-level. Depending on our goals, we may choose to model differently the inter and intra-subject variability of records. To perform group analysis, single-subject brain images are typically registered to a common template (the MNI space) [65], so as to reduce the variability in brain shape. Even though this leads to a loss in anatomical information, this approach is motivated by the fact that brain networks are often located within well defined anatomic regions that are shared across subjects, modulo some non-rigid transformation. This work does not focus on inter-subject variability, and will assume that brain images arise from a distribution that is shared across subjects, once they have been registered to the MNI space.

2.3.4. Resting-state Functional Magnetic Resonance Imaging (rs-fMRI)

Resting-state fMRI data is a popular and cost-effective way to acquire functional MRI data. During a resting-state scan, the subject is asked to do nothing in particular, and the BOLD signal is acquired. This process yields unlabelled data, as there is no specific task or stimuli provided to the subject. This data can be thought of as brain movies, with one image per second and between 50,000 to 200,000 voxels per image. Resting-state scans are widely available and are the cheapest way to acquire fMRI data. For example, the Human Connectome Project [66] provides 4,000 records of 15-minute resting-state scans across 1,000 subjects. The UK BioBank [67] initiative is also gathering resting-state fMRI data for 100,000 subjects.

Although resting-state fMRI data is unlabelled, it contains a lot of intrinsic information about brain functioning. As such, it is central in modern fMRI analysis and is reviewed briefly in the thesis. Resting-state fMRI data can be used to study functional connectivity between brain regions and to identify functional networks in the brain. It has also been used to study differences in brain function between healthy individuals and those with neurological or psychiatric disorders. Overall, resting-state

fMRI data is a valuable tool for studying brain function and has the potential to provide insights into a wide range of neurological and psychiatric conditions.

Resting-state fMRI data contains valuable information about the brain's functional networks, which are spatial regions that tend to activate together. These networks can be used to reduce the dimensionality of the signal from 105 voxels to a few hundreds components without loosing cognitive information.

Historically, functional networks uncovered from resting-state data have been used to construct biomarkers for certain diseases, such as Alzeimer disease [68], Parkinson disease [69], autism spectrum disorder [70], Attention Deficit Hyperactivity Disorder (ADHD) [71]. It has also been shown to be related to behavior, e. g., fluid intelligence [72]. More precisely, the time correlation structure between the various functional networks is often of interest to better understand how the brain of a single subject functions. These correlations can be estimated in the framework of functional connectivity [73], that is still being refined [74].

Recently, many studies have also demonstrated the interest of using resting-state data to better frame inter-subject variability in more complex protocols involving controlled stimuli [75]. At a more fundamental level, resting-state analysis is central to better understand the role of functional networks in cognition. For example, the default-mode network [76] is a pre-eminent network in resting-state that tends to activate during mind-wandering, while the amygdala [77] is a brain region partly responsible for emotional responses.

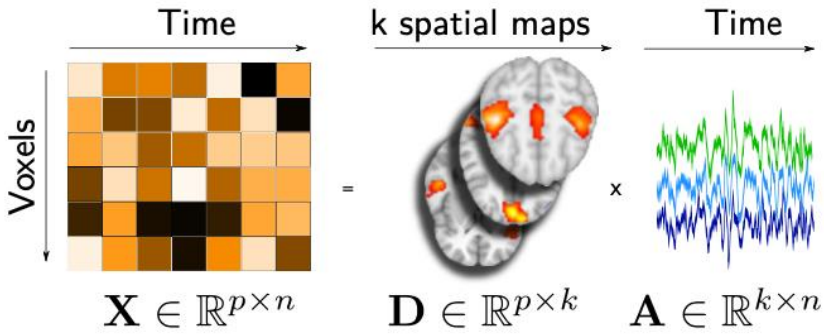

Figure 2.3 Modelling of the brain signal in resting-state fMRI

(The data matrix writes as a product of two matrices that yield spatial and temporal information respectfully).

CHAPTER 3. METHODOLOGY

In this chapter, I report the methodology used in this thesis for the classification and detection of ASD. Section 3.1 presents the general pipeline of the methodology applied in this thesis. The following sections: Section 3.2, Section 3.3, Section 3.4 provides the detailed workflow of each step in general pipeline of the thesis' methodology, which are data preprocessing, feature extracting, classification using machine learning and deep learning, respectively. Finally, Section 3.5 presents the cross-validation process.

3.1. Thesis Workflow

Rs-fMRI performs brain mapping to evaluate the connections between brain regions in a resting state. Studies mainly use raw fMRI image data, but raw data requires a lot of processing time and can lead to overfitting issues due to high dimensionality. To address this issue, machine learning methods are applied to detect autism spectrum disorders from functional connectivity networks extracted from preprocessed fMRI data. The general pipeline for predictive analysis of brain connectivity based biomarkers is illustrated in Figure 3.1.

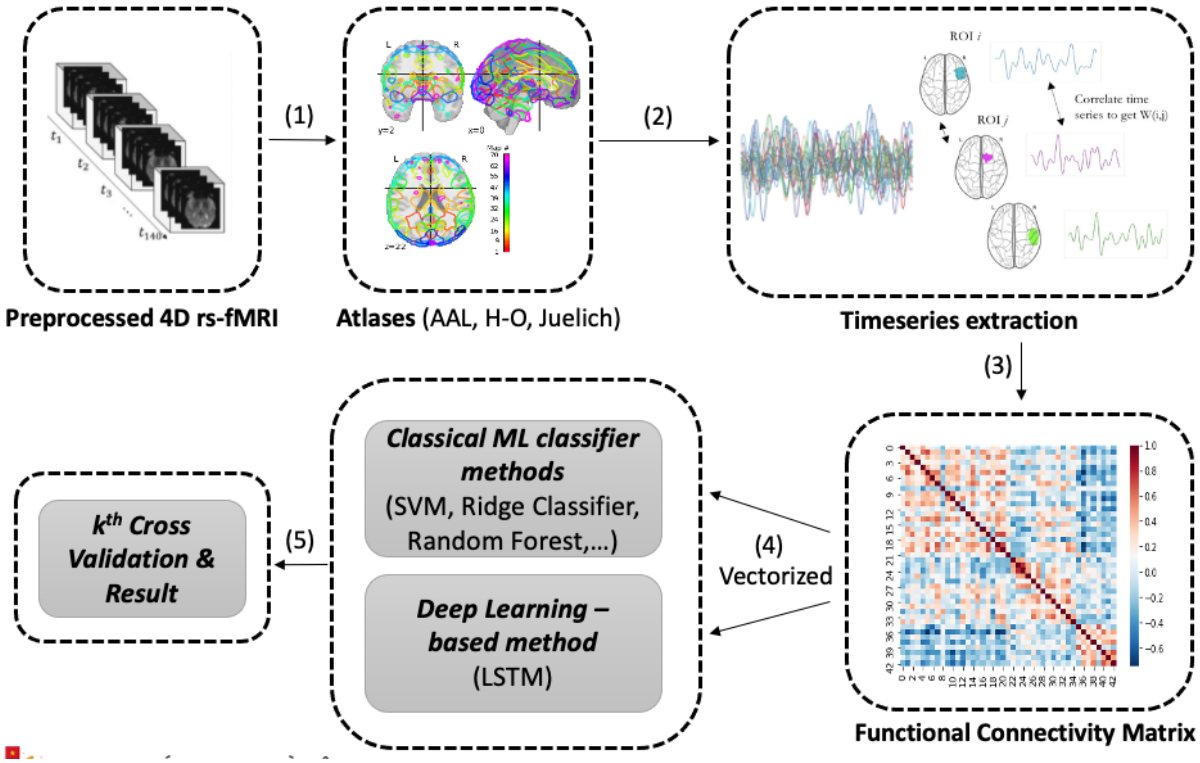

Figure 3.1 Methodology framework for ASD classification

As illustrated in Fig. 3.1, Functional connectivity matrices are extracted from preprocessed rs-fMRI data as follows:

(1) A parcellation of the brain is defined on preprocessed rs-fMRI data of ASD and TC subjects

(2) The time series corresponding to the voxels in each region of the parcellation are aggregated into one representative time series often by averaging

(3) The connectivity matrix of ROIs (2D) is built by computing the similarity or correlation among the representatives of each pair of regions in the parcellation based on the average of the time-series of the rs-fMRI data. The connectivity matrix is then used as the raw data for classification processes which may involve feature extraction/selection. Feature selection involves the selection of specific connections that may become identified as biomarkers.

(4) Functional connectivity matrix is then vectorized (1D) to reduce data dimensionality and then use for classification

(5) Predictive performance is estimated by the training/testing of classification models often in a cross-validation process.

Prediction performance may be influenced by the choices made at each step of the workflow, particularly by the choice of brain parcellation, the functional connectivity matrix estimation procedure, and the classification model building algorithm. After the cross-validation assessment, the cross-validation classification performance results may be used to identify biomarkers in the connectivity matrix.

3.2. Dataset

3.2.1. Preprocessing Pipeline

The MRI scans are extremely sensitive and even a slightest change in the parameters could greatly affect the captured data. The rs-fMRI data is collected while the subject is awake and conscious inside the MRI machine. This increases the possibility of the subject moving their head inside the machine. This possibility along with multiple other factors can result in a variation between the data captured and the original information. The MRI data may get corrupted due to several causes like movement of the subject while scanning the brain, presence of noise in the scanner, variation in the shape and size of the brain of each subject, time required to capture the information and so on. In order to reduce the effect of noise or artifacts on the captured data some basic spatial and functional preprocessing methods are required to be executed before extracting any information from them.

The preprocessing methods that are essential to be applied to the rs-fMRI data include: spatial normalization, motion correction (realignment), time slice correction [78]. Once the data has been preprocessed to remove any artifacts or noise the data is then analyzed to extract the desired information.

Spatial normalization: The size and shape of the human brain varies from subject to subject. While performing segmentation or extracting features each point in one brain should lie in the same location in another brain, to analyze or extract the same region for all the subjects. This also prevents the neural network to learn on their individual shape and sizes. Therefore, all the brains must be modified to a standard shape and size using a predefined standard template. This helps the model to select region of interests uniformly and reduce the effect of distortion.

Motion correction: rs-fMRI dataset usually contains scans from subjects with their age ranging. It is difficult for all the subjects to lie perfectly still while the scans are being captured. This results in a change in alignment of the brain over the multiple scans of the same individual. To reduce this noise component, a process to correct this motion is performed. The process involves selecting one of the brain volumes of the subject as the reference volume and then aligning the data present in all the volumes of that subject to the reference volume. This reference volume selected was the center scan. The realignment of the brain takes place by using three dimensional parameters and 3 rotational parameters to move the data.

Slice time correction: The resting state functional MRI data for each subject includes scans that capture the time series information. Each scan is to be recorded at a particular point in time to obtain the BOLD information for the same instant. However, it requires some time to obtain information for each slice in a volume. Therefore, the data captured at different layers of the brain are obtained at different time points. In order to resolve this problem slice time correction is performed. Slice time correction method calculates the Fourier transform of the signal at each voxel to convert the signal of that slice of the brain into a sum of scaled and phase shifted sine waves of each voxel. After which these converted signals are moved forward or backward depending on the interpolation. These values are interpolated between the values of the points that were actually sampled to obtain a value that would mimic the voxel value that would have been captured at that time instant.

3.2.2. Preprocessed ABIDE dataset

A central role in the effort to obtain reproducible biomarkers is played by the availability of public datasets, such as the Autism Brain Imaging Data Exchange (ABIDE) dataset [79] that includes demographic, clinical information and data from several magnetic resonance imaging (MRI) modalities allowing for a variety of studies such as brain maturity estimation as a biomarker of brain abnormality. ABIDE is a multisite platform that has aggregated functional and structural brain imaging data collected from 17 different laboratories around the world. The ABIDE dataset includes functional and structural brain imaging data collected from laboratories around the world to ensure data diversity and to understand the complexity of the disease to be

able to make the diagnosis at earlier ages, to select optimal treatments and to predict outcomes.The preprocessed connectomes project (PCP) from the ABIDE has openly released 539 individuals who have ASD and 573 TD to the public [80]. These 1112 datasets consist of structural and preprocessed resting state functional MRI data along with phenotypic information. The rs-fMRI data are slice time corrected, motion corrected and normalized. In this study, all rs-fMRI data are selected from the CPAC preprocessing pipeline and band-pass filtered (0.01 - 0.1Hz). From these 1112 subjects, 1035 subjects are screened for our study since only 1035 subjects have been given the corresponding completed phenotypic information, which is essential for our further study. In these 1035 subjects, there are 505 ASD and 530 TD, 157 females and 878 males. The summary information of the screened subjects is displayed in Table 3.1. Table 3.1 contains the key phenotypical information of ASD and TD such as gender, age and lab site ID.

Table 3.1 Preprocessed ABIDE dataser phenotypical information

Site	ASD	TC	M	F	Age Range
CALTECH	19	18	29	8	17 ~ 56
CMU	14	13	21	6	19 ~ 40
KKI	20	28	36	12	8 ~ 13
LEUVEN	29	34	55	8	12 ~ 32
MAX_MUN	24	28	48	4	7 ~ 58
NYU	75	100	139	36	6 ~ 39
OHSHU	12	14	26	0	8 ~ 15
OLIN	19	15	29	5	10 ~ 24
PITT	29	27	48	8	9 ~ 35
SBL	15	15	30	0	20 ~ 64
SDSU	14	22	29	7	9 ~ 17
STANFORD	19	20	31	8	8 ~ 13
TRINITY	22	25	47	0	12 ~ 26
UCLA	54	44	86	12	8 ~ 18
UM	66	74	113	27	8 ~ 29
USM	46	25	71	0	9 ~ 50
YALE	28	28	40	16	7 ~ 18
TOTAL	**505**	**530**	**878**	**157**	**6 ~64**

3.3. Feature Extraction

3.3.1. Brain Atlases/Parcellations

The brain atlas in an anatomic label map which is used to divide and label region of interests (ROIs) in the brain. Korbinian Brodmann subdivided the cerebral cortex into numerous areas based on regional differences in the distribution, density, shape, and size of cell bodies [81] providing one of the first brain anatomical parcellation allowing researchers to investigate brain-behavioral associations with developmental [82], cognitive, and clinical phenotypes [83]. Brain atlases are applied in order to obtain the region representative time series for each of the regions of the selected parcellations. The parcellation scheme, also called atlas, is used to segment the entire brain into smaller cortical and subcortical anatomical units, i.e., groups of voxels, also called regions of interest (ROIs).

As discussed in [84] there are several approaches to the definition of the brain parcellation which may lead to significant differences in the computational experiments outcomes [85]. One kind of brain atlas is the anatomically guided parcellations such as the Tailarach and Tournoux (TT), Eickhoff-Zilles [86], Harvard Oxford (HO) [87], and the Automated Anatomical Labeling (AAL) [88] defined from the brain segmentation of selected control populations. Another type are brain atlases produced from the segmentation of the rs-fMRI time series of the brain volume using clustering techniques, such as the Craddok [89] parcellations. All these atlases are defined at the conventional resolution of sMRI of $1mm^3$.

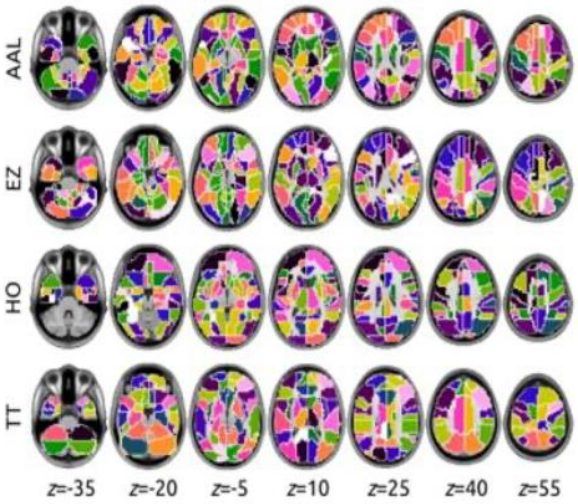

Figure 3.2 Different types of atlas and theirs regions of interest (ROIs)

In this research project, to analyze the functional connectivity of the brain, the brain atlases presented in Table 3.2 were used to extract time series data representing each selected brain region.

Table 3.2 Brain atlases with total number of ROIs

Atlas	ROIs
Automated Anatomical Labelling (AAL)	116
Harvard-Oxford (H-O)	48
Juelich	121

(1) **AAL - Automated Anatomical Labelling**: The AAL atlas is distributed with the AAL Toolbox. AAL atlas is used to partition the GM maps into 116 brain anatomical regions.

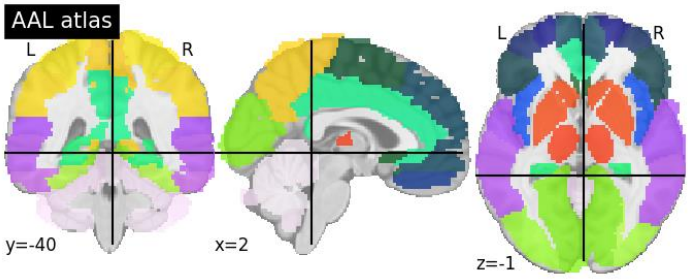

Figure 3.3 AAL atlas

(2) **H-O – Harvard-Oxford**: The Harvard-Oxford (HO) atlas was developed at the Center for Morphometric Analysis (CMA), and distributed with the FMRIB Software Library (FSL). It comes with a probability distribution for each brain region obtained from a Maximum A posteriori (MAP) estimate. The HO atlas is split into cortical and subcortical probabilistic atlases. A 25% threshold was applied to each of these atlases and they were subsequently bisected into left and right hemispheres at the midline (x = 0). ROIs representing left/right WM, left/right GM, left/right CSF and brainstem were removed from the subcortical atlas.

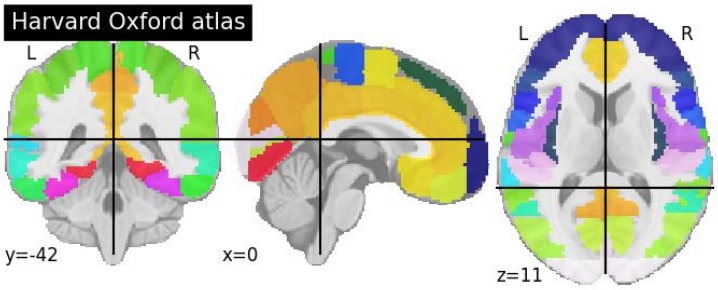

Figure 3.4 Harvard-Oxford atlas

(3) **Juelich**: The Julich-Brain Atlas [90] contains cytoarchitectonic maps of more than 200 areas of the human brain including cortical areas and subcortical nuclei. It depicts differences in distribution, density and morphology of cells in a three-dimensional space in probabilistic maps that reflect the variability between individual brains. The Julich-Brain serves as a basis for spatially aligning and annotating data and knowledge from different levels of brain organisation such as connectivity, molecular architecture or functional brain segregation and is a powerful tool to help researchers and clinicians better interpret images of individual brains.

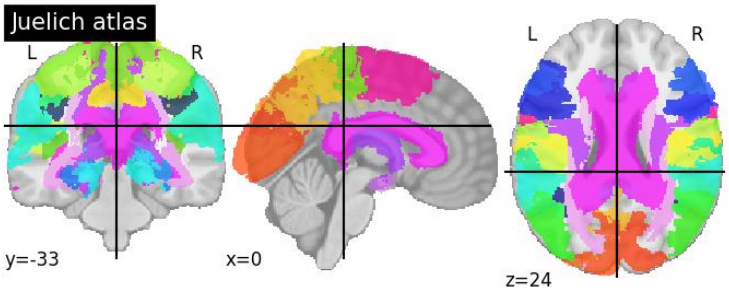

Figure 3.5 Juelich atlas

3.3.2. Time Series

Rs-fMRI data contains multiple scans of the slices of the brain taken over time. The data collected is used to track any change in the neurological activity of a subject. Once the rsfMRI data is pre-processed to reduce noise and remove unnecessary artifacts, the desired atlas is superimposed on it. The atlas will segment the data into Regions-of-Interest (ROIs). Then the average intensity value of each region is calculated and used as the value representing that ROI, which is denoted as timeseries.

The common procedure to extract the time course of one ROI is to take the average of all voxel BOLD signals within that region. Thus, each ROI can be represented by a distinct time-course. Then, the rs-fMRI imaging data can be described as an $R \times T$ matrix, where R denotes the number of ROIs and T is the length of the time course, i.e., the number of time points in the BOLD signal.

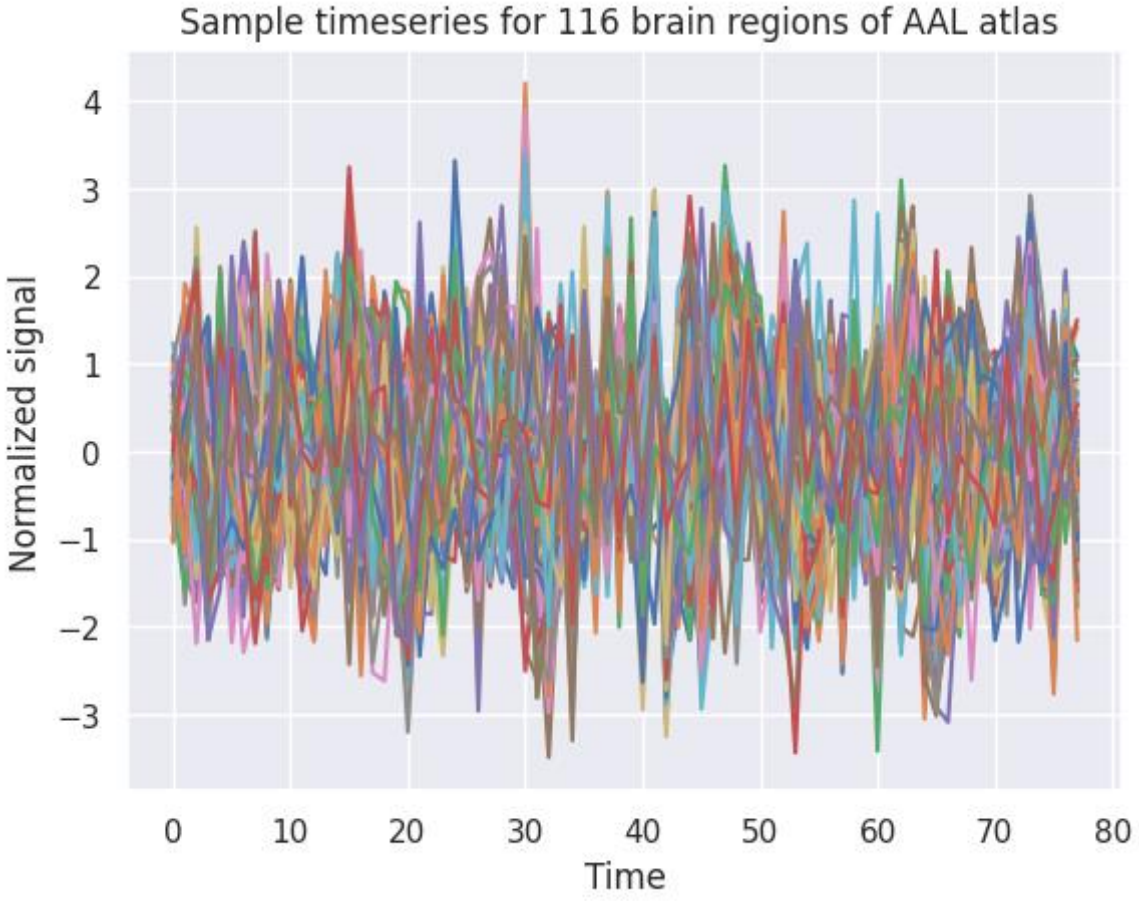

Figure 3.6 Sample timeseries signals

3.3.3. Functional Connectivity (FC)

Functional MRI measures the BOLD signal - a measure associated with neuronal activity - across the entire brain in order to identify functional characteristics of the brain [91]. One particular type of analysis that describes the functional organization of the brain is functional connectivity analysis. Functional connectivity (FC) is denoted as a matrix with the rows and columns representing nodes and each element of the matrix representing the edge strength or functional connection between the corresponding nodes. Functional connectivity characterizes how in-sync, or out-of-sync, particular regions are by correlating their BOLD responses at every time point

across an entire fMRI scan. The rationale is that regions that are highly correlated in their BOLD responses at a given time are likely to be working together for a particular task or activity. These correlation values are stored in what is known as a connectivity matrix. Each position in the matrix represents the correlation of BOLD activity between two particular regions [92].

The connectivity matrices are constructed according to the following connectivity measures:

- The covariance matrix computed using the Ledoit-Wolf shrinkage estimator [93]
- The Pearson Correlation Coefficient (PCC) [94] among each pair of ROI time series, which is computed as the normalization of the covariance matrix
- The precision computed as the inverse of the covariance matrix
- The partial correlation obtained regressing out all other connections for each pair of regions [95]
- The tangent space representation of the matrices obtained by whitening them [96].

Although Pearson correlation coefficient is the simplest and most commonly used for defining edge strength, it is not indicative of the direct connection. Partial correlation, on the other hand, is used to estimate the direct connection, which is achieved by regressing out possible indirect connections through other nodes. Using realistic simulated fMRI data, partial correlation was shown to be one of the best methods for network connection detection with high sensitivity compared with various other network models.

From these functional connectivity matrices, scientists can then examine properties that describe the inter-relatedness of many regions. These properties can be used to identify network-level inter-individual differences in a large cohort.

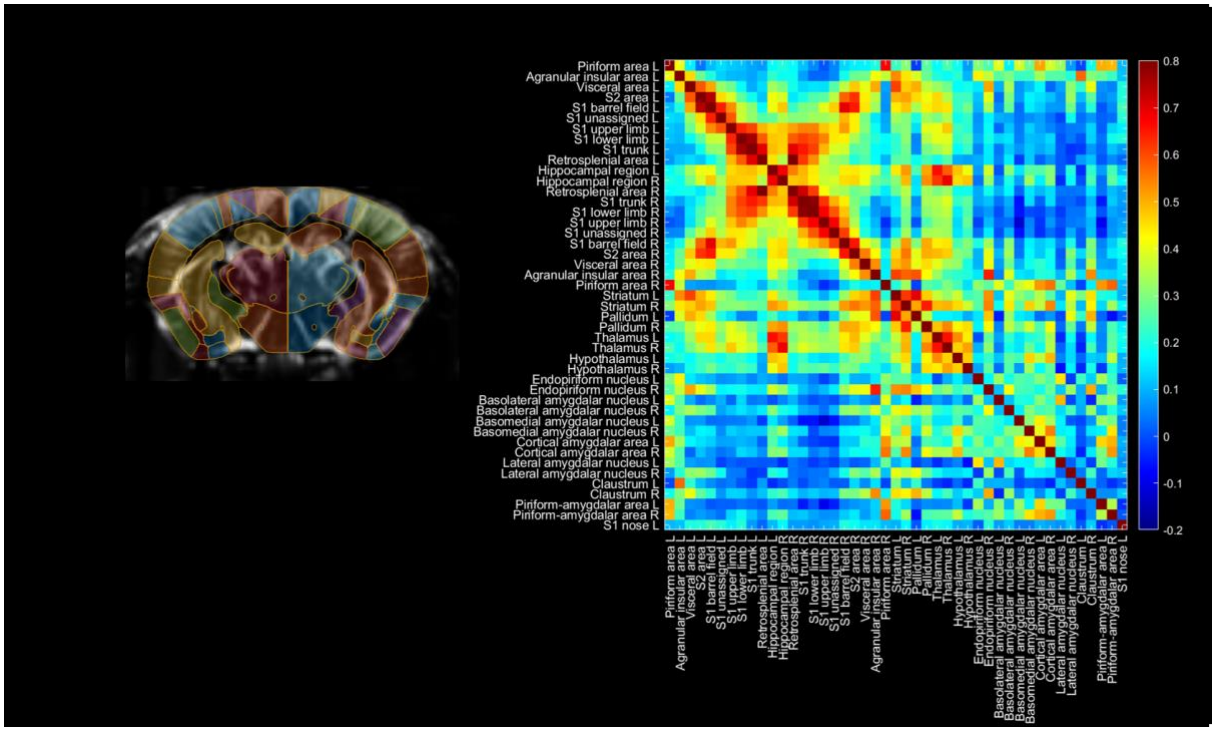

Figure 3.7 2D resting-state functional connectivity shows local and inter-hemispheric correlations in a mouse model

The anatomical label map divides the brain into different region of interests depending on the atlas used. Once the brain is divided, the connectivity information between these regions is to be calculated. This is done by calculating the average value of all of the voxel present in a ROI and then representing that ROI with the averaged value. This process is repeated for all the scans taken at different points in time. Once the average value representing all the ROIs is calculated then the correlation value between the ROIs is calculated to obtain the connectivity matrix. The correlation values range from -1 to 1, with -1 indicating that the two ROIs are inversely correlated and 1 indicating that the ROIs are highly correlated.

The basic idea was to analyze the BOLD values of each voxel and if the voxels had intensities which were highly correlated and the voxels were in two different ROIs then the two ROIs were said to be connected. This graph representation of FC is also called as ”connectome” , which describes the topological characteristics of the brain network. Consequently, graph theory and complex network analysis or feature extraction algorithms are utilised to extract features for further analysis.

In this thesis, Pearson's correlation coefficient is the used measurement for constructing functional connectivity networks.

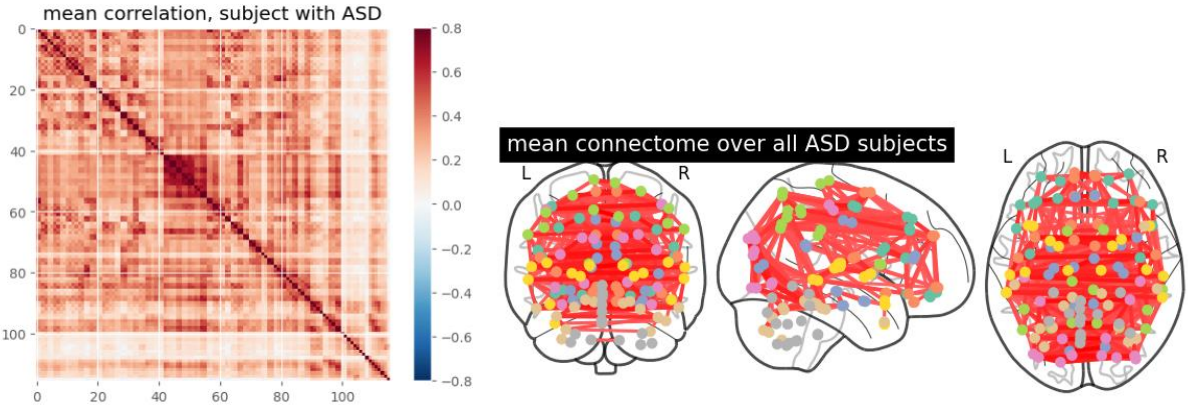

Figure 3.8 Functional connectivity matrix of ASD subject

3.4. Machine Learning-based Classification

Machine learning techniques have obtained prominent achievements in the analysis of rs-fMRI brain image. Supervised machine learning techniques have been widely used for the classification of patients versus typical controls. In this thesis, for running machine learning algorithms, the preprocessed data with Pearson correlation coefficient, graph measures, and intensity averages used as features was divided in a 80:20 ratio for training and test. classifier building methods that are available from the open and free-source Python library scikit-learn v0.22 (https://scikit-learn.96.org/) were used. Specifically, following machine learning classifiers were ultilized: Support Vector Classifier, Ridge Classifier, Decision Tree, Random Forest and Naive Bayes. In terms of Support Vector Classifier, this thesis used the linear kernel version because its response is more stable, needs less parameter tuning, and is more efficient computationally. Additionally, both sparse (*l1*) and nonsparse (*l2*) regularization terms are considered.

3.4.1. Support Vector Classifier

Support Vector Classifier (SVC) [97] is a machine learning algorithm that looks for the maximum margin hyperplane to separate two classes of samples. It solves a linear programming problem to determine the relevance of the samples to the class boundary. Linear kernel version of the SVC was used because it is more stable, requires less

parameter tuning, and is more computationally efficient. In some instances, this thesis also carry out a variable selection procedure based on their statistical significance in an ANOVA analysis [98]. Both sparse (*l1*) and non-sparse (*l2*) regularization terms were considered in this thesis.

Support Vector Machines (SVM) were developed by Vapnik [99] and have gained popularity due to their promising features, such as better empirical performance. The formulation uses the Structural Risk Minimization (SRM) principle, which has been shown to be superior to traditional Empirical Risk Minimization (ERM) principle used by conventional neural networks. SRM minimizes an upper bound on the expected risk, whereas ERM minimizes the error on the training data. This difference equips SVM with a greater ability to generalize, which is the goal in statistical learning. SVMs were originally developed to solve classification problems but have recently been extended to solve regression problems.

3.4.2. Ridge Classifier

Ridge Classifier (RC) [100] treats the classification problem as a straightforward regression in the [−1, 1] interval with a penalty on the size of the coefficients. The ridge coefficients minimize a penalized residual sum of squares,

$$\hat{\beta}^{ridge} = argmin \left\{ \sum_{i=1}^{N} \left(y_i - \beta_0 - \sum_{j=1}^{p} x_{ij} \beta_j \right)^2 + \lambda \sum_{j=1}^{p} \beta_j^2 \right\} \tag{3.1}$$

Here $\lambda \geq 0$ is a complexity parameter that controls the amount of shrinkage: the larger the value of λ, the greater the amount of shrinkage. The coefficients are shrunk toward zero (and each other). The idea of penalizing according to the sum of squares of the parameters is also used in neural networks, where it is known as weight decay. An equivalent way to write the ridge problem is

$$\hat{\beta}^{ridge} = argmin \sum_{i=1}^{N} \left(y_i - \beta_0 - \sum_{j=1}^{p} x_{ij} \beta_j \right)^2 \tag{3.2}$$

which makes explicit the size constraint on the parameters. When there are many correlated variables in a linear regression model, their coefficients can become poorly determined and exhibit high variance. A wildly large positive coefficient on one variable can be canceled by a similarly large negative coefficient on its correlated cousin. By imposing a size constraint on the coefficients, this problem is alleviated.

The ridge solutions are not equivariant under scaling of the inputs, and so one normally standardizes the inputs before solving Equation 3.1. In addition notice that the intercept β0 has been left out of the penalty term. Penalization of the intercept would make the procedure depend on the origin chosen for Y; that is, adding a constant c to each of the targets y_i would not simply result in a shift of the predictions by the same amount c. It can be shown that the solution to Equation 3.1 can be separated into two parts, after reparametrization using centered inputs: each x_{ij} gets replaced by $x_{ij} - \bar{x_j}$. We estimate $\beta_0 by \bar{y} = \frac{1}{N}\sum_1^N y_i$. The remaining co-efficients get estimated by a ridge regression without intercept, using the centered x_{ij} . Henceforth we assume that this centering has been done, so that the input matrix X has p (rather than $p + 1$) columns.

Ridge regression can also be derived as the mean or mode of a posterior distribution, with a suitably chosen prior distribution. In detail, suppose $y_i \sim N(\beta_0 + x_i^T\beta, \sigma^2)$, and the parameters β_j are each distributed as $N(0, \tau^2)$, independently of one another. Then the (negative) log-posterior density of β, with τ^2 and σ^2 assumed known, is equal to the expression in curly braces in eq. 3.1, with $\lambda = \sigma^2/\tau^2$. Thus the ridge estimate is the mode of the posterior distribution; since the distribution is Gaussian, it is also the posterior mean.

3.4.3. Decision Tree

Decision Tree [101] is a non-parametric supervised learning algorithm, which is utilized for both classification and regression tasks. It has a hierarchical, tree structure, which consists of a root node, branches, internal nodes and leaf nodes. A decision tree starts with a root node, which does not have any incoming branches. The outgoing branches from the root node then feed into the internal nodes, also known as decision nodes. Based on the available features, both node types conduct evaluations to form homogenous subsets, which are denoted by leaf nodes, or terminal nodes. The leaf nodes represent all the possible outcomes within the dataset.

Decision tree learning employs a divide and conquer strategy by conducting a greedy search to identify the optimal split points within a tree. This process of splitting is then repeated in a top-down, recursive manner until all, or the majority of records

have been classified under specific class labels. Whether or not all data points are classified as homogenous sets is largely dependent on the complexity of the decision tree. Smaller trees are more easily able to attain pure leaf nodes—i.e. data points in a single class. However, as a tree grows in size, it becomes increasingly difficult to maintain this purity, and it usually results in too little data falling within a given subtree. When this occurs, it is known as data fragmentation, and it can often lead to overfitting. As a result, decision trees have preference for small trees, which is consistent with the principle of parsimony in Occam's Razor; that is, "entities should not be multiplied beyond necessity." Said differently, decision trees should add complexity only if necessary, as the simplest explanation is often the best. To reduce complexity and prevent overfitting, pruning is usually employed; this is a process, which removes branches that split on features with low importance. The model's fit can then be evaluated through the process of cross-validation. Another way that decision trees can maintain their accuracy is by forming an ensemble via a random forest algorithm; this classifier predicts more accurate results, particularly when the individual trees are uncorrelated with each other.

3.4.4. Random Forest

Random Forest [102] is a supervised learning algorithm and a popular ensemble method that combines by majority voting the response from a committee of decision trees trained upon bootstrapped versions of the training data. The "forest" it builds, is an ensemble of decision trees; usually trained with the "bagging" method. Moreover, the variables used to compute each node split are randomly selected. The basic premise of the algorithm is that building a small decision tree with few features is a computationally cheap process [103]. A tree-based model involves recursively partitioning the given dataset into two groups based on a certain criterion until a predetermined stopping condition is met. At the bottom of decision trees are the leaf nodes where the decision on the class is performed. Figure 3.9 illustrates a recursive partitioning of a two-dimensional input space with axis-aligned boundaries. Each time the input space is partitioned in a direction parallel to one of the axes. In the figure, the first split is defined by $x2 \geq a2$. Then, the two resulting subspaces are partitioned: The left branch corresponds to the split on $x1 \geq a4$. The right branch is first split by the rule $x1 \geq a1$, and then one of its subbranches is split by the ryle $x2 > a3$.

Depending on how the partition and stopping criteria are set, decision trees can be designed for both classification tasks (categorical outcome, for example, logistic regression) and regression tasks (continuous outcome).

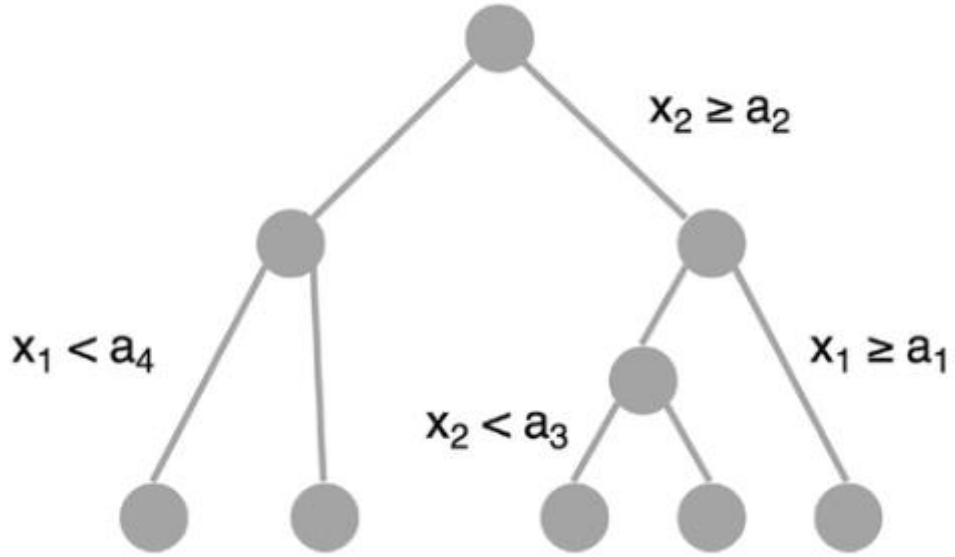

Figure 3.9 Graphical representation of a binary decision.

For both classification and regression problems, the subset of predictor variables selected to split an internal node depends on predetermined splitting criteria that are formulated as an optimization problem. A common splitting criterion in classification problems is entropy, which is the practical application of Shannon's source coding theorem that specifies the lower bound on the length of a random variable's bit representation. At each internal node of the decision tree, entropy is given by the equation (3.3) where c is the number of unique classes and pi is the prior probability of each given class. This value is maximized to gain the most information at every split of the decision tree. For regression problems, a commonly used splitting criterion is the mean squared error at each internal node:

$$E = -\sum_{i=1}^{c} p_i \times \log(p_i) \tag{3.3}$$

A drawback of decision trees is that they are prone to overfitting, which means that the model follows the idiosyncrasies of the training dataset too closely and performs poorly on the test data, i.e. unknown data at training time. Overfitted decision trees lead to low generalization performance.

Individual decision trees are easily interpretable, but this interpretability is lost in random forests because many decision trees are aggregated. However, in exchange, random forests often perform much better on prediction tasks. The random forest algorithm more accurately estimates the error rate compared with decision trees. More specifically, the error rate has been mathematically proven to always converge to zero as the number of trees increases [104].

The error of the RF is approximated by the out-of-bag error during the training process, wich is computed as follows. Each decision tree is built on a different bootstrap sample. Each bootstrap sample randomly leaves out a number of the observations in the original sample. These left-out observations for a given tree are referred to as the out-of-bag sample. Finding parameters that would produce a low out-of-bag error is often a good strategy for model selection and parameter tuning. Note that in the RF algorithm, the size of the subset of predictor variables strongly determines the final depth of the trees. Hence, it is a parameter that needs to be tuned during model selection.

3.4.5. Naive Bayes

Naive Bayes [105] assumes the statistical independence of the features, so that the classifier can be built as an aggregation of one dimensional not interacting classifiers modeled by a loose mixture of Gaussians. Naive Bayes is used widely in many applications such as: text categorization, document judgement and data stream classification. Naive Bayes is a generative model based classifier [106] with a fast learning and testing process.

Bayesian classifiers are straightforwardly derived from the Bayes rule and probability theorems. It has been proven that learning the optimal Bayesian classifier from training data is an NP-hard problem. A simplified version of Bayesian classifier called naive Bayes uses two assumptions. The first is that attributes are conditionally independent given the class label. The second is that, no latent attribute affects the label prediction process [107].

Assume, the vector $(x_1, \ldots, x_n)$ represents the n attributes of the instance x. Let it be c the class label of the instance x. The probability of observing x given the class label c can be computed by as follows:

$$p(x_1, \ldots, x_n|c) = \prod_{i=1}^{n} = p(x_i|c) \quad (3.4)$$

The conditional independence assumption between the attributes in Naive Bayes is weak, and rarely correct in most real problems except of situations in which the attributes are extracted from independent stochastic processes. Some methods have been introduced for improving the conditional independence assumption in Naive Bayes.

3.5. Deep Learning-based Classification using LSTM

3.5.1. Introduction on LSTM

LSTM [108] is a popular and recent recurrent neural network and has recently been used for ASD classification. This thesis works on the ASD classification using the LSTM-based framework.

To understand LSTM model, first, we must understand the evolution of a Recurrent Neural Network (RNN) [109] from a basic neural network. The structure of the basic neural network can be broken down into three components: input layer, hidden layer, and output layer. The Perceptron is the first trainable neural network and the simplest neural network with only one layer with adjustable weights and thresholds lying between input and output layers. RNN is a type of neural network that deals explicitly with time series or sequential data. RNNs are the improvements of the Feed-Forward Neural Networks (FFNN), where the signals can travel only one way from input to output. FFNNs can only read the current input layer and lacks an internal memory; therefore, these are bad at predicting what is to come. The most widely studied and used feed-forward neural network model is the multilayer FFNN, also called multilayer perceptrons. RNNs are called recurrent because they perform the same task for every element of a sequence, with the output being dependent on the previous computations. RNN is better than FFNN in modeling sequential data because RNN has a memory that captures the information about what has been calculated so far, and the output from the previous steps is taken as an input for the current stage. Hence, RNN makes a prediction, or a decision, based on its current input and the outputs from the previous step.

Mathematically speaking, the basic version of RNN has the form $h_t = g(Wx_t + W_h h_{t-1} + b)$, where x_t is the k dimensional input vector at time t, h_t the $d-$dimensional hidden state, g is the activation function (such as the logistic function, the hyperbolic tangent function, or the rectified Linear Unit), and $W \in \mathbb{R}^{d\times k}$, $W_h \in \mathbb{R}^{d\times d}$ are weight matrices, and $b \in \mathbb{R}^{d\times 1}$ is a bias vector [110]. As we can see, RNN is revolutionary compared to FFNNs, but there are some limitations. In the normal RNN cell, the input at a time step and the hidden state from the previous time step is passed through the activation function to obtain a new hidden state and output where the gradients carry information used in the RNN parameter update. The parameter updates become insignificant when the gradient tends to zero, which means no real learning is done. On the other hand, when the error gradients accumulate during an update, the explosion occurs through exponential growth by repeatedly multiplying gradients through the network layers with values larger than 1, resulting in large gradients. These, in turn, result in large updates to the network weights and an unstable network. Hence due to the vanishing or exploding nature of the (stochastic) gradients with long sequences, RNN has difficulty in learning long-term dependencies [111]. For this reason, a different and improved architecture of RNNs was created called, LSTM.

LSTM essentially extends the memory of RNNs so that it can handle longer sequences of information. Unlike a standard RNN, which is comprised of the input, hidden, and output layers, LSTM has a memory cell that consists of an input gate, forget gate, and an output gate [112]. The most crucial component of LSTM architecture is the cell state which runs through the chain, with only linear interaction and keeping the flow of information unchanged. The gate mechanism of LSTM deletes or modifies the information of the cell state. First, the input gate decides which information is received, and then it goes through the forget gate, which determines if it is essential information to keep, and then it makes its way to the output gate. The LSTM utilizes a sigmoid function, a tanh function, and a pointwise multiplication operation to decide which information is passed through based on its importance.

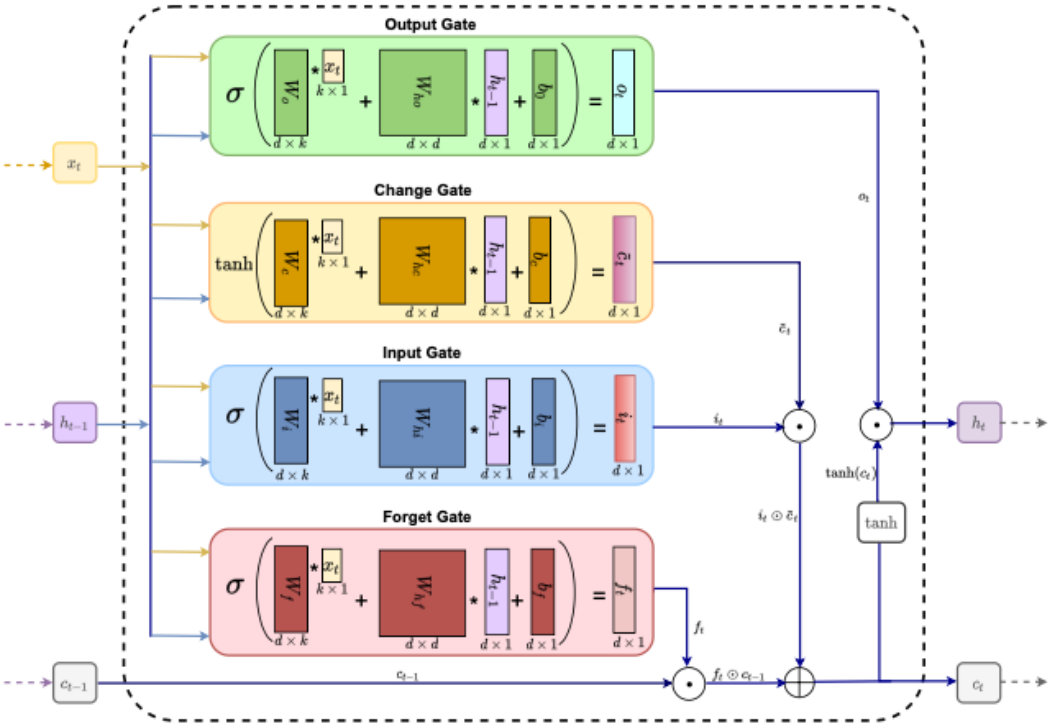

Figure 3.10 Long Short-term Memory (LSTM) architecture.

The architecture of LSTM at time t is presented in the Fig. 3.10. In this figure, the four gates - output, change, input, and forget - are shown with their operations at time t. For a given input sequence $\{x_1, x_2, \ldots, x_n\}$, $x_t \in \mathbb{R}^{k\times 1}$ is the input sequence at time t. The memory cell c_t updates the information using three gates: input gate i_t, forget gate f_t, and change gate $\tilde{c}_t$. The hidden state h_t is updated using output gate o_t and the memory cell c_t. The respective gates and layers compute the following functions at time t:

$$i_t = \sigma(W_i x_t + W_{hi} h_{t-1} + b_i)$$

$$f_t = \sigma(W_f x_t + W_{hf} h_{t-1} + b_f)$$

$$o_t = \sigma(W_o x_t + W_{ho} h_{t-1} + b_o)$$

$$\tilde{c}_t = tanh(W_c x_t + W_{hc} h_{t-1} + b_c)$$

$$c_t = f_t \odot c_{t-1} + i_t \odot \tilde{c}_t$$

$$h_t = o_t \odot tanh(c_t)$$

where, σ represent the sigmoid function. The operator $\odot$ is the element-wise product, $W \in \mathbb{R}^{d\times k}$, $W_h \in \mathbb{R}^{d\times d}$ are weight matrices, and $b \in \mathbb{R}^{d\times 1}$ are bias vectors. Furthermore, n, k, d denotes the sequence length, the number of features, and the

hidden size respectively [117]. In addition, to incorporate the required dimension of LSTM architecture, the input sequence X_t is created by taking m continuous sequence $x_t : x_{t+m-1}$ which is a matrix of shape $k \times m$ for $t \in \{1,2,\ldots,n-m-1\}$. The output h_t of LSTM is a feature representation for the input sequence X_t at time t. Mathematically, h_t can be expressed as follows:

$$h_t = LSTM(X_t, h_{t-1}, c_{t-1}, w)$$

where w denotes all learnable parameters. Since the final hidden state h_f encodes the most information from the input sequence, it is converted to a vector using a dense layer.

3.5.2. Overfitting Issues of LSTM model

Overfitting is a common problem in machine learning and deep learning, and LSTM models are no exception [113]. In particular, by overtraining when the training data are insufficient or the number of features is relatively large, the training effectof the model may be better, but the test or verification effect may be poor. A similar error result with overfitting was observed, as displayed in Figure 3.11. While the training error decreased with the increasing iterations, the verification error began to increase gradually after decreasing to a certain number of iterations.

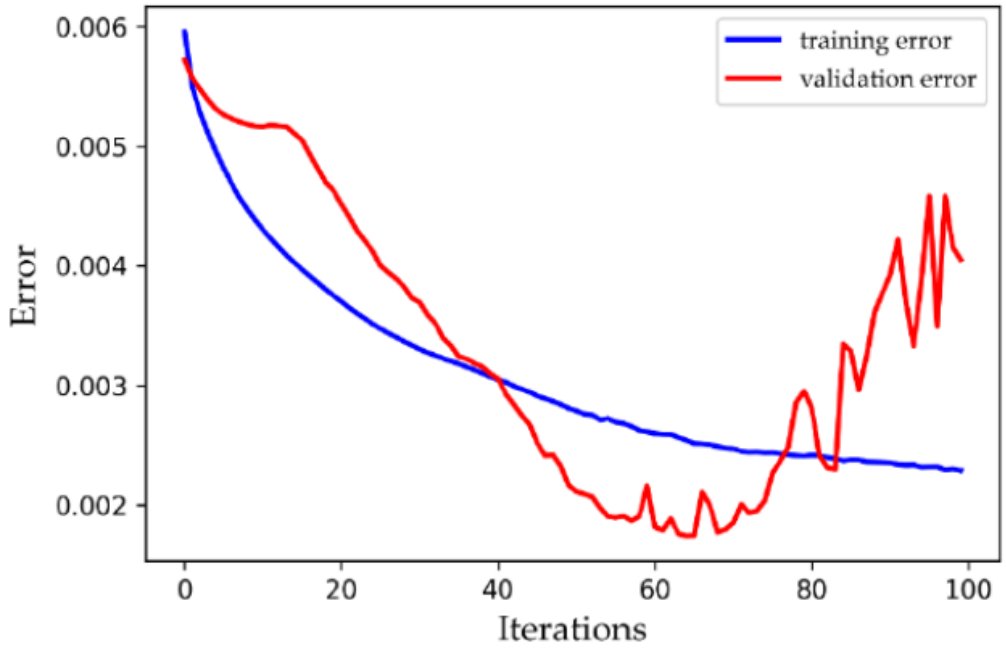

Figure 3.11 An example of overfitting

In order to enhance the generalization ability of deep learning models, overfitting must be avoided. The main approaches are L1 and L2 regularization, data augmentation, feature selection, dropout, etc. Regularization is the addition of a constraint to the cost function to reduce some parameters. Dataaugmentation is a way to increase training samples and expand the dataset. Feature selection meanschoosing an approach to select the most influential feature and reducing irrelevant features. This paperadopts dropout, one of the most commonly-used methods in deep learning, to prevent overfitting inthe neural network. The key idea of dropout is to drop units (along with their connections) from theneural network randomly during training to prevent units from co-adapting too much.

3.5.3. Architecture used: LSTM with Dropout Layers

This thesis designs an LSTM model with dropout to predict ASD. As mentioned previously, our rationale for using LSTM is its ability to remember inputs over a long period, making it possible to remember data sequences. ASD detection aims to identify a group of samples which deviate markedly noticeably from the existing data. That is why LSTM was chosen to identify and accurately predict ASD from rs-fMRI which is a long series of sequential data.

The LSTM architecture utilizes three types of layers: input, hidden and output. The hidden layers are fully connected to the input and output layers. A layer in LSTM is composed of blocks and each block has three gates: input, output and forget, which are all interconnected. These gates decide whether to let new input in (input gate), delete the information because it is not important (forget gate) or allow it to impact the output at the current time step (output gate). The neural network here uses a structure with a three-layer hidden layer to achieve higher accuracy of the model. Dropout layers introduced earlier are used to prevent overfitting. The Rectified Linear Unit (Relu) function was selected as the activation function between the hidden layers. The Relu function can be expressed as Equation 3.5, and the value range of the function is greater than 0:

$$f(x) = \begin{cases} 0, & x < 0 \\ x, & x \geq 0 \end{cases} \tag{3.5}$$

Compared with the sigmoid activation function of a traditional artificial neural network, Relu can avoid predicting negative concentration values and is superior to other activation functions interms of statistical performance and computational cost. Binary Cross-Entropy was chosen as the loss function. For the optimizer, Adam optimizer was used for training process. The structure of the LSTM prediction model with dropout is shown in Fig. 3.12.

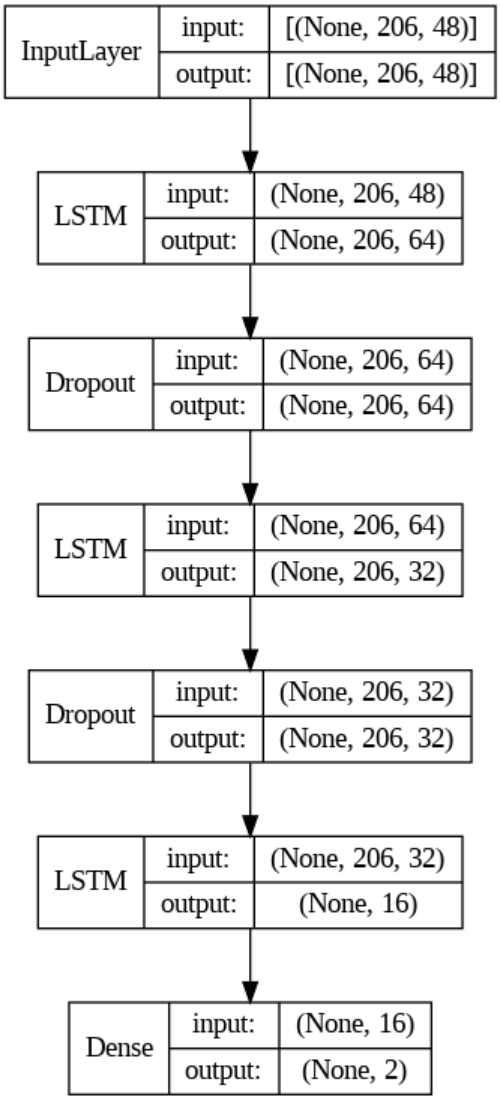

Figure 3.12 The structure of the LSTM model with dropout layers for ASD prediction

As illustrated in Fig. 3.12, the data must be reshaped to develop the LSTM input layer, which needs the input data to be 3-dimensional: that is, training sample, time step and features. For this layer, an activation function (ReLu) was added. In our proposed model, the dropout was applied between the hidden layers and between the last hidden layer and the output layer. The dropout was set at 40%, as recommended in the literature [114].

The last layer (dense layer) defines the number of outputs which represent the classes. The output is considered as a vector of integers, which is converted into a binary matrix. The ASD prediction is formulated as a binary-classification problem which requires the creation of 2 output values, one for each class.

3.6. Cross Validation

Cross validation is statistical technique for evaluating and comparing learning algorithms by dividing the dataset into two segments: one used to learn or train the model and other used to validate the model [115]. In k-fold cross validation schema, dataset is segmented into k equally sized portions, segments or folds. Subsequently, k iterations of learning and validation are performed, within each iteration (k−1) folds are used for learning and a different fold of data is used for validation. Upon completion of k folds, performance of an algorithm is calculated by averaging values of evaluation metric i.e. accuracy of each fold.

In this thesis, extracted features from rs-fMRI were evaluated on Stratified 10-fold cross validation scheme. The dataset is divided into 10 folds of equal portions. In 10-fold cross validation, 9 folds of data are used for training purpose and the other one portion is used for testing purpose. In stratified cross-validation, the folds are made by preserving the percentage of samples for each class. Fig. 3.13 illustates the process of 10-fold cross validation. The 10-fold cross validation procedure produces ten results, and these results can be averaged to obtain the final performance estimation.

$$performance = \frac{1}{10}\sum_{i=1}^{10} performance_i \tag{3.2}$$

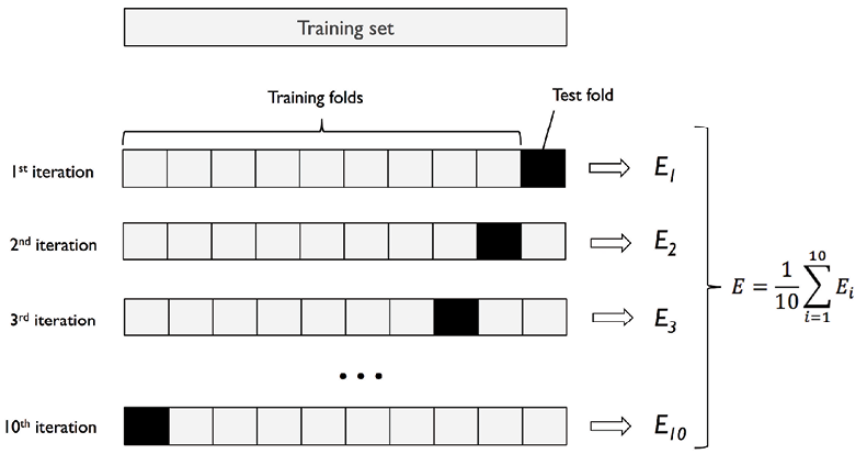

Figure 3.13 10-fold cross validation

CHAPTER 4. RESULTS AND DISCUSSION

In this chapter, I present the experimental results of a various combination of choices in the design of ASD detection using rs-fMRI. Section 4.1 describes the performance evaluation metrics used in result analysis. Section 4.2 shows feature extraction results of timeseries signal and FC matrix with the top correlated brain regions in ASD and TC subjects. Section 4.3 provides the ASD detection results with machine learning classifiers. Section 4.4 presents deep learning-based results using LSTM model.. Finally, the best results are compared with the state of art and some general remarks are given in Section 4.5.

4.1. Evaluation Metrics

To investigate the effectiveness of the model with the test dataset, different evaluation metrics can be used to evaluate different machine learning algorithms. For classification problems, the commonly used performance metrics include accuracy, precision, recall, sensitivity, specificity and receiver operating characteristic (ROC) cure, area under curve (AUC), etc. Definition of the terms are explained below:

- Positive (P): Observation is positive. If we were predicting the presence of a disease, “P” would mean the observation has the the disease.
- Negative (N): Observation is not positive. “N” means the observation doesn’t have the the disease.
- True Positive (TP): Observation is positive, and is predicted to be positive. “TP” means a disease subject is predicted as a disease subject.
- False Negative (FN): Observation is positive, but is predicted to be negative. “FN” means a disease subject is predicted as a normal subject.
- True Negative (TN): Observation is negative, and is predicted to be negative. “TN” means a disease subject is predicted as a disease subject.
- False Positive (FP): Observation is negative, but is predicted to be positive. “FP” means a normal subject is predicted as a disease subject.

Accuracy in classification problems is the number of correct predictions made by the model over all kinds predictions made.

$$Accuracy = \frac{TP + TN}{N}$$

Precision is a measure that tells us what proportion of patients that we diagnosed as having ASD, actually had ASD.

$$Precision = \frac{TP}{TP + FP}$$

Recall or sensitivity is a measure that tells us what proportion of patients that actually had ASD was diagnosed by the algorithm as having ASD.

$$Recall = \frac{TP}{TP + FN}$$

Specificity is a measure that tells us what proportion of patients that did not have ASD, were predicted by the model as not ASD. F-measure (or F1-score) is the harmonic mean of the precision and recall. It always be nearer to the smaller value of precision or sensitivity.

$$F1 - score = 2\ \frac{Precision \times Recall}{Precision + Recall}$$

The ROC curve is the most commonly used way to visualize the performance of a binary classifier, and AUC summarizes its performance in a single number between 0 and 1 (ideal classifier). An ROC curve illustrates in a binary classifier system the discrimination threshold created by plotting the true positive rate vs. false positive rate. ROC curves typically feature true positive rate on the Y axis, and false positive rate on the X axis. The ROC is a plot of sensitivity vs. (1 – specificity), and the area under the curve shows how well a method makes positive and negative categorical distinctions. A larger area under the curve (AUC) is usually better. ROC is a probability curve and AUC represents degree or measure of separability. It tells how much model is capable of distinguishing between classes. The higher the AUC, the better the model is at distinguishing between patients with disease and no disease. In this study, the sensitivity represents the proportion of ASDs correctly predicted, while the specificity describes the proportion of TCs correctly predicted.

4.2. Feature Extraction Results

4.2.1. Timeseries Extraction

The rs-fMRI Nifti data can be extracted into timeseries signal from different ROIs after masking brain atlases or brain parcellations on raw data using Nilearn library in Python. Figure 4.1, 4.2 and 4.3 is the sample timeseries extracted of an ASD subject using three brain atlases icluding AAL, HO and Juelich, respectively. The timeseries graphs below have x-axis corresponding to the number of timespoint in rs-fMRI scan, y-axis corresponding to the average value of each brain region and the different color lines corresponding to the brain regions masked, which are 116 ROIs for AAL atlas, 48 ROIs for HO atlas and 121 ROIs for Juelich atlas.

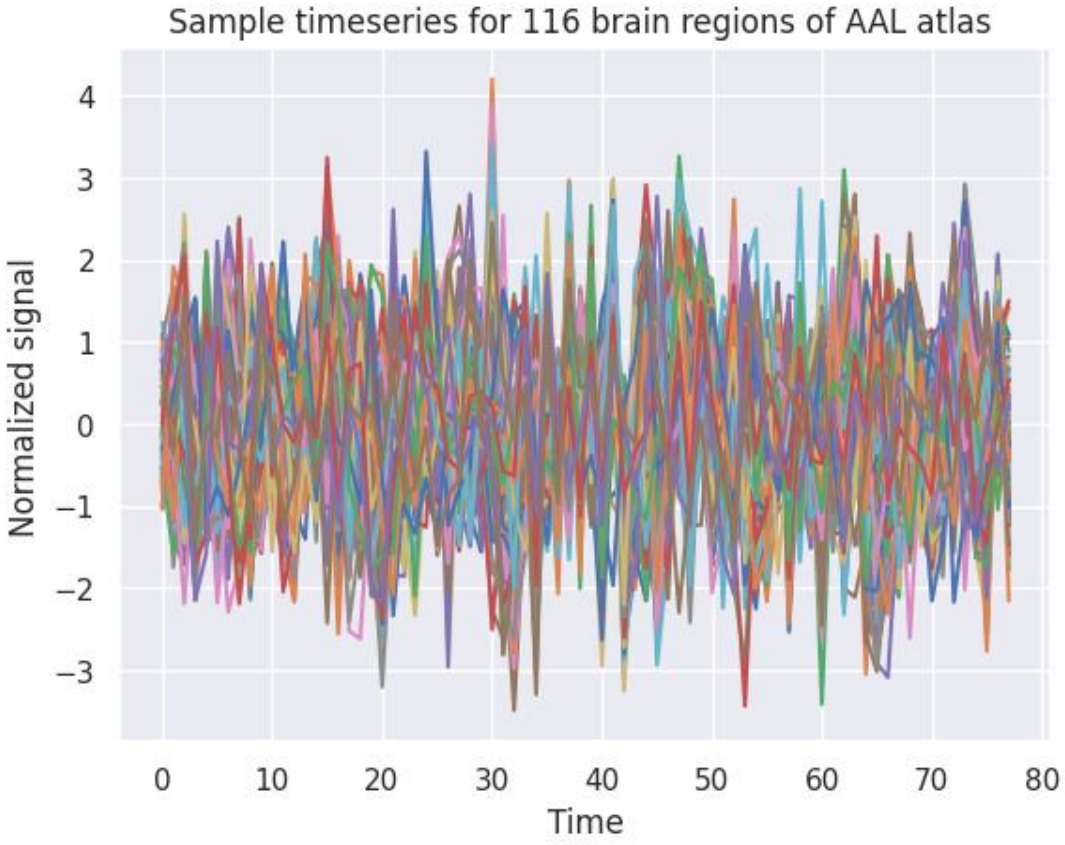

Figure 4.1 Sample timeseries signals of an ASD subject using AAL atlas

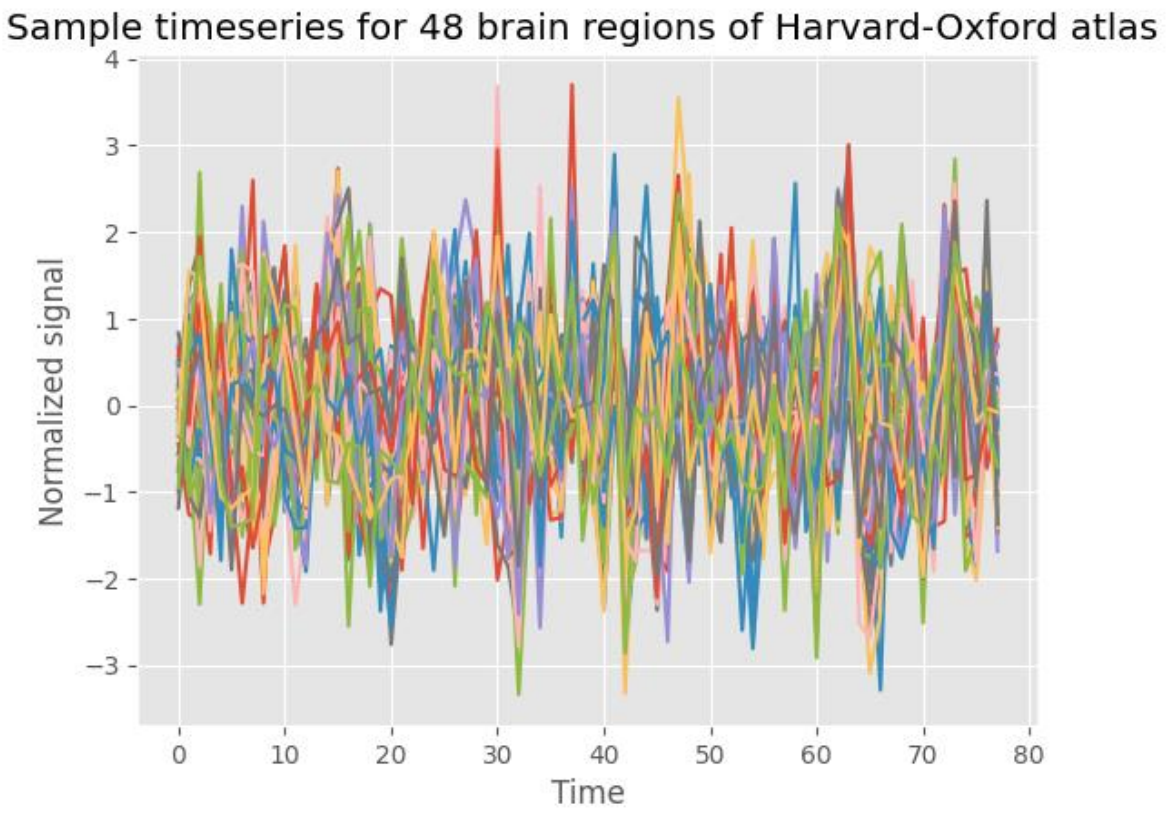

Figure 4.2 Sample timeseries signals of an ASD subject using HO atlas

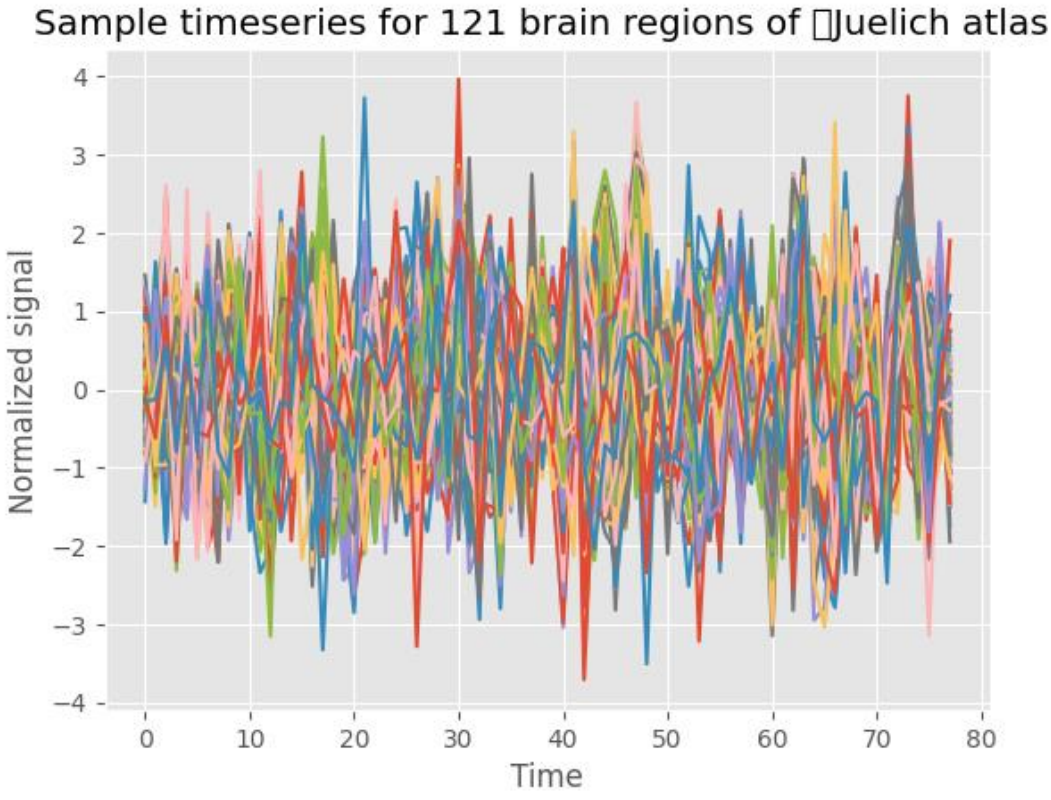

Figure 4.3 Sample timeseries signals of an ASD subject using HO atlas

4.2.2. Functional Connectivity Matrix Extraction

This thesis used Pearson's correlation coefficient measurement for constructing functional connectivity matrix. The results of FC matrix extraction from rs-fMRI data using three brain atlases: AAL, HO and Juelich are displayed in the following subsections. The below figures presents the functional connectivity matrices of three first ASD subjects, mean functional connectivity and connectome of all ASD subjects. The comparison of functional connectivity matrix of an ASD and TC subject is also considered. The size of FC matrices correspond to the number of ROIs masked using AAL, HO and Juelich atlas, which are 116×116, 48×48 and 121×121, respectively.

4.2.2.1 FC using AAL atlas

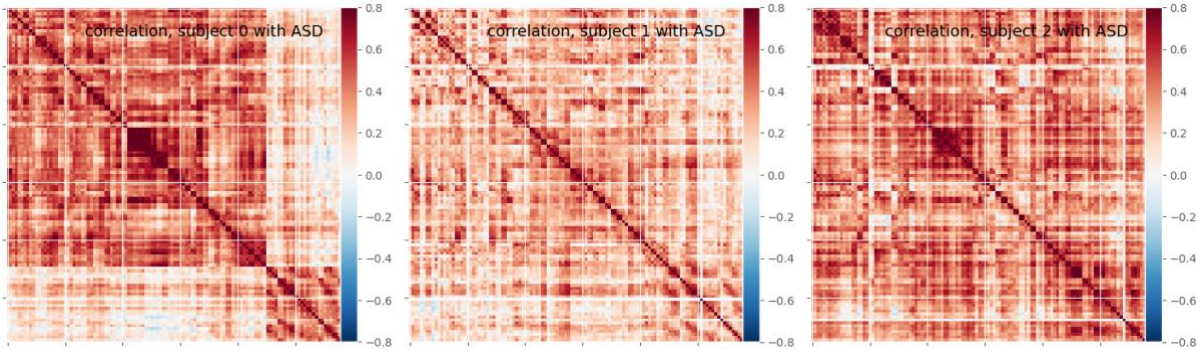

Figure 4.4 Sample functional connectivity matrices of 3 first ASD subjects (AAL atlas)

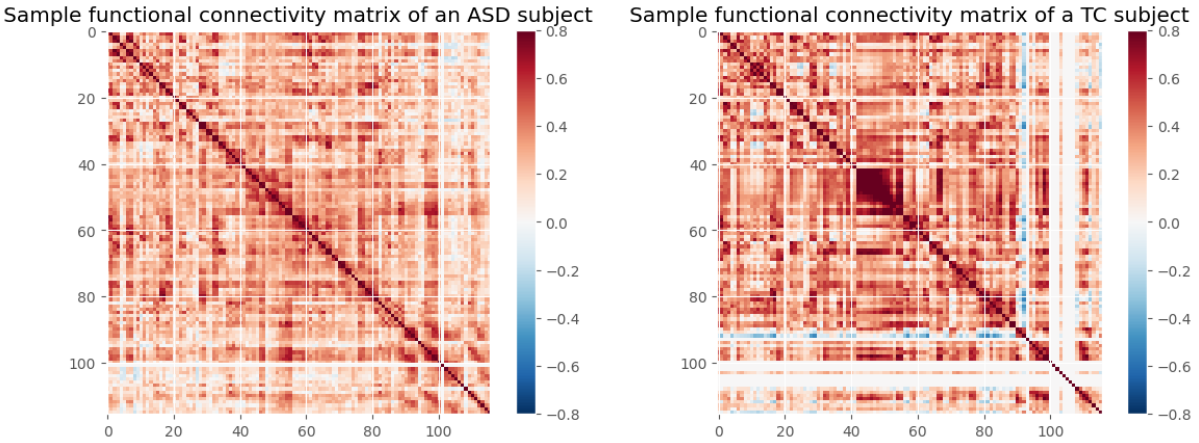

Figure 4.5 Comparison of functional connectivity matrices of an ASD and a TC subjects (AAL atlas)

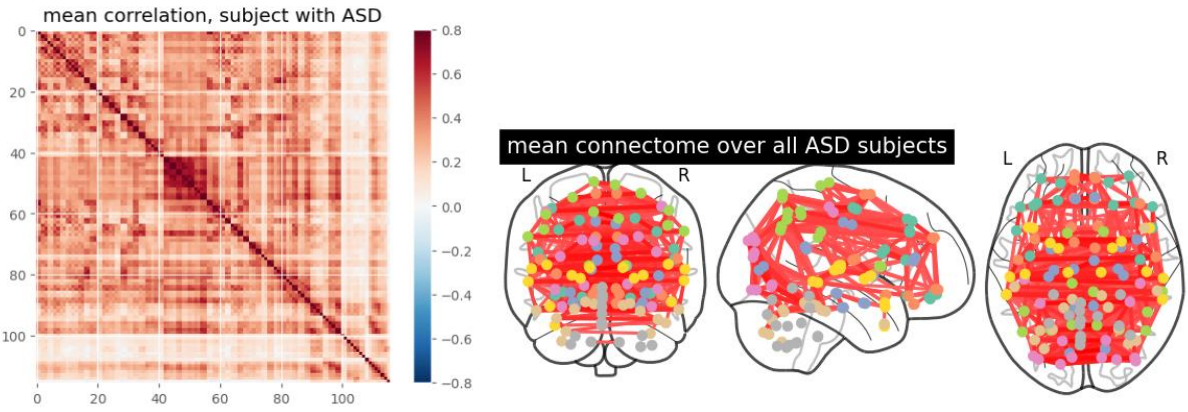

Figure 4.6 Mean functional connectivity matrix of all ASD subjects (AAL atlas)

4.2.2.2 FC using HO atlas

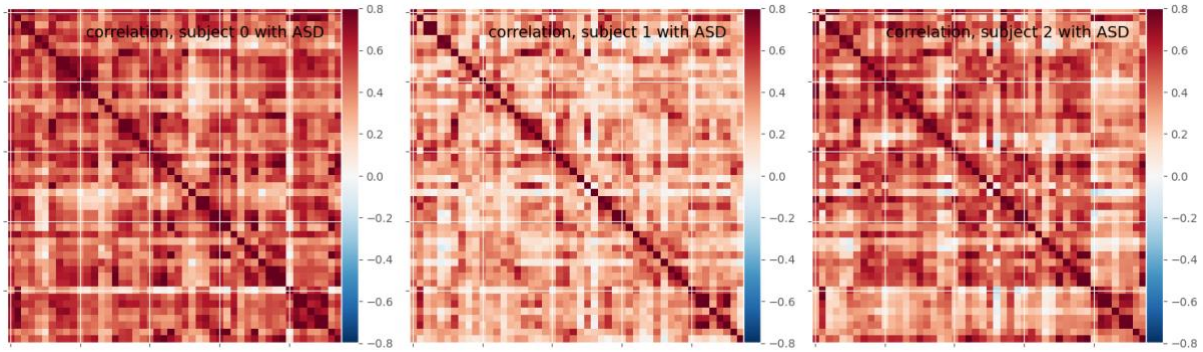

Figure 4.7 Sample functional connectivity matrices of 3 first ASD subjects (HO atlas)

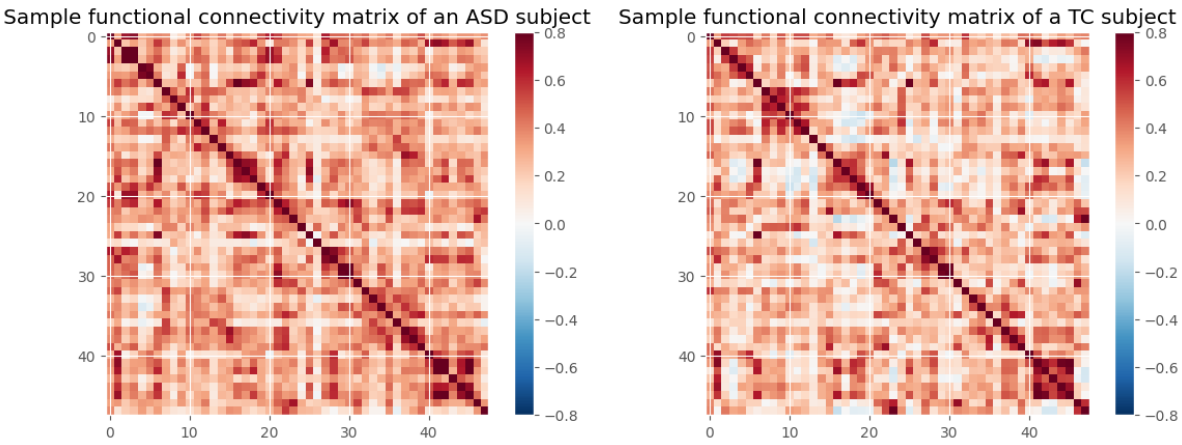

Figure 4.8 Comparison of functional connectivity matrices of an ASD and a TC subjects (HO atlas)

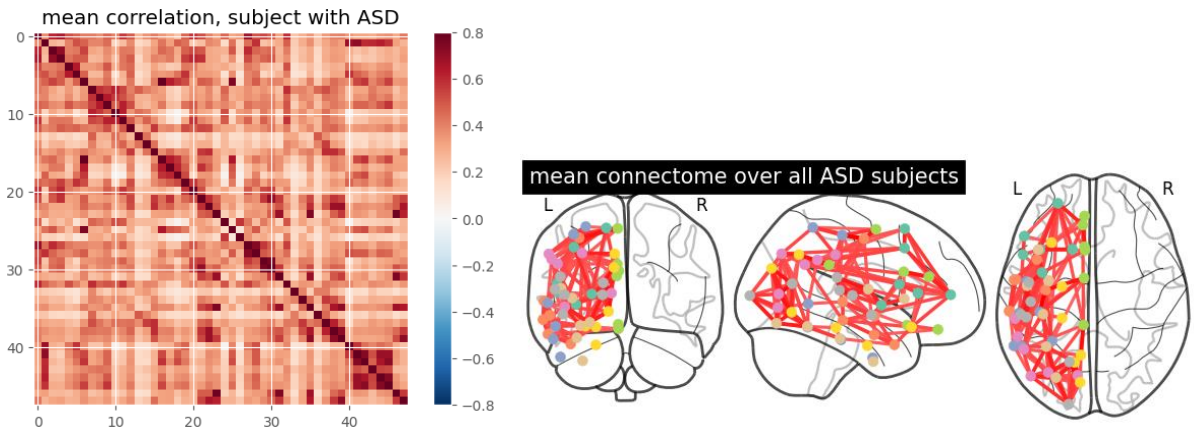

Figure 4.9 Mean functional connectivity matrix of all ASD subjects (HO atlas)

4.2.2.3 FC using Juelich atlas

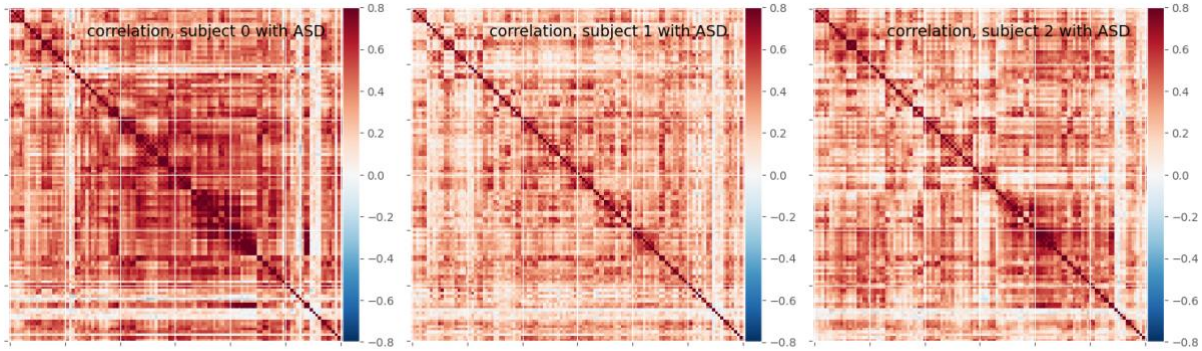

Figure 4.10 Sample functional connectivity matrices of 3 first ASD subjects (Juelich atlas)

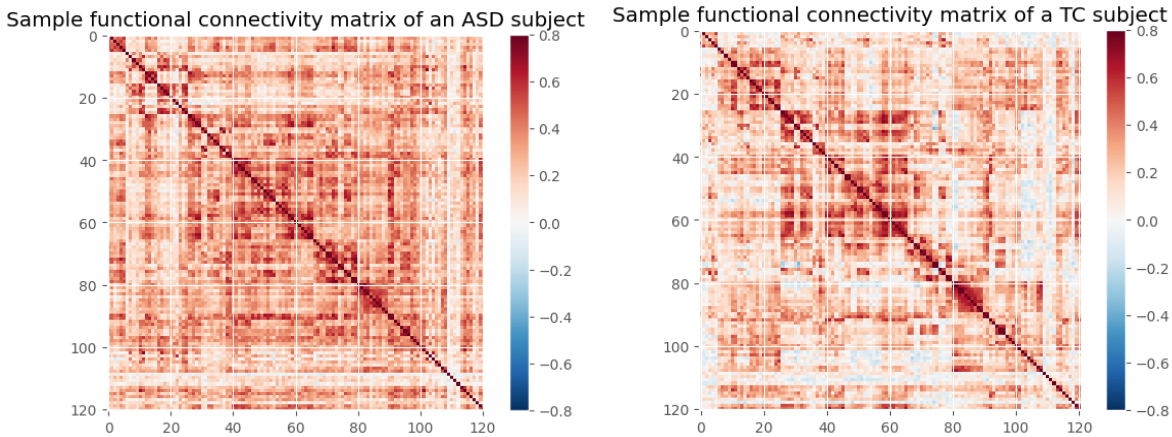

Figure 4.11 Comparison of functional connectivity matrices of an ASD and a TC subjects (Juelich atlas)

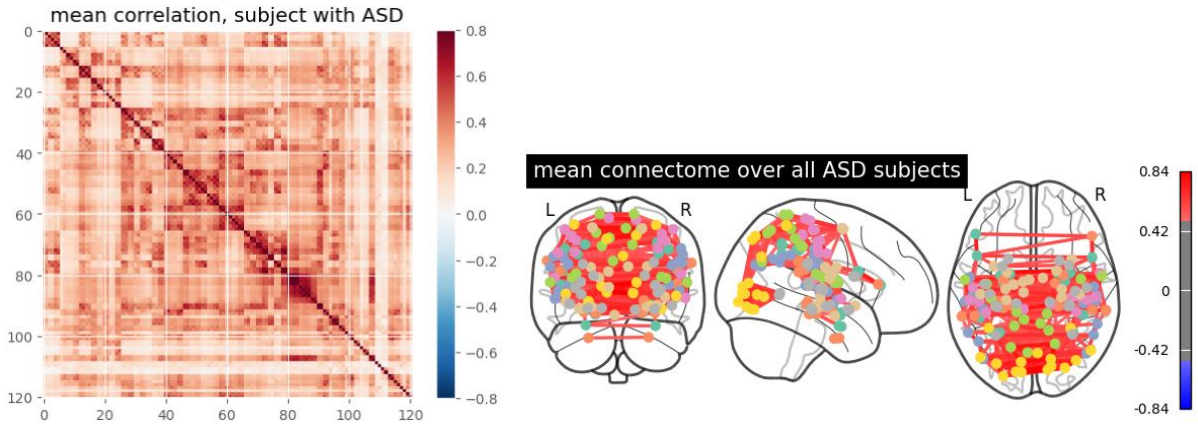

Figure 4.12 Mean functional connectivity matrix of all ASD subjects (Juelich atlas)

4.2.3. Top Functional Correlated Brain Regions of ASD and TC

In Table 4.1, the top five correlated ROIs from the Juelich atlas for the ASD group and TD group are listed. These selected ROIs are selected according to the mean of the connectivity matrix for each group.

Table 4.1 Top 5 correlated ROIs of ASD and TC subject

ASD	Right Calcarine Gyrus ⇔ Right Lingual Gyrus
	Left Lingual Gyrus ⇔ Left Cerebelum
	Right Precuneus ⇔ Right Cingulate Gyrus
	Right Cuneus ⇔ Left Cuneus
	Right Calcarine Gyrus ⇔ Left Calcarine Gyrus
TC	Right Calcarine Gyrus ⇔ Right Lingual Gyrus
	Right Precuneus ⇔ Right Cingulate Gyrus
	Left Precuneus ⇔ Left Cingulate Gyrus
	Right Calcarine Gyrus ⇔ Left Calcarine Gyrus
	Right Cuneus ⇔ Left Cuneus

ASD is a developmental brain disorder that affect social interaction, verbal and nonverbal communication. Many research work have highlighted ASD with a deficit in the integration of cognitive mechanisms. Related fMRI studies have showed that ASD

are characterized by reduced functional connectivity throughout the cortical language systems [116]. This thesis also supported this view. The highly correlated Left Cerebelum and Left Lingual Gyrus ROIs are only found in ASD. The highly correlated Left Precuneus and Left Cingulate Cortex are only found in TC participants.

4.3. Machine Learning-based Results

4.3.1. Training Settings

This thesis was implemented on Google Colab using Python v3.6. The cloud provided a free TPU and 12.72 GB of RAM on an Intel Core i7 processor. The machine learning model used the Keras API with TensorFlow as a supporting program. To evaluate the model, scoring and calculation methods from the *scikit-learn* library were used.

For all machine learning classifiers, the ten-fold cross-validation method was used to find the best value of the hyperparameters. SVC was implemented with l_1, l_2. For the Random Forest classifier, the maximum depth of the tree between 5 and 20, the number of trees between 500 and 2500, and the node impurity criterion gini and entropy were compared, and the model with 2500 trees and the maximum depth of 5 were fitted using gini coefficient to minimize the node impurity. All classifiers were performed with a learning rate of 0.001 and a batch size of 50.

4.3.2. Experimental Results

In this thesis, three brain atlas including AAL, Harvard-Oxford and Juelich were ultilized for defining ROIs and extracting features. The input for the models is the features extraction obtained using Pearson correlation method for constructing FC. We applied and compared six different traditional machine learning classifiers for the classification of ASD and TD. ten-fold cross-validation is performed on the whole data to develop the classification model. The average performance metrics for different classifiers with 10-fold cross validation are presented in the following tables. The values for accuracy, F1-score, precision, recall, ROC-AUC, and mean absolute error were evaluated for the effectiveness of each atlas. All average cross-validation results

are displayed in Table 4.2, 4.3, 4.4 and illustrated by graphs for comparison in Figure 4.13, 4.14 and 4.15.

Table 3.2 Performance results using AAL atlas

	SVC L2	SVC L1	Ridge Classifier	Decision Tree	Random Forest	Naïve Bayes
Accuracy	0.620	0.570	**0.640**	0.470	0.510	0.560
F1-score	0.638	0.572	**0.660**	0.473	0.516	0.574
Precision	0.653	0.615	**0.678**	0.396	0.582	0.557
Recall	**0.640**	0.560	**0.640**	0.480	0.560	**0.640**
ROC_AUC	0.652	0.584	**0.656**	0.490	0.576	0.584
MAE	0.390	0.430	**0.380**	0.470	0.470	0.440

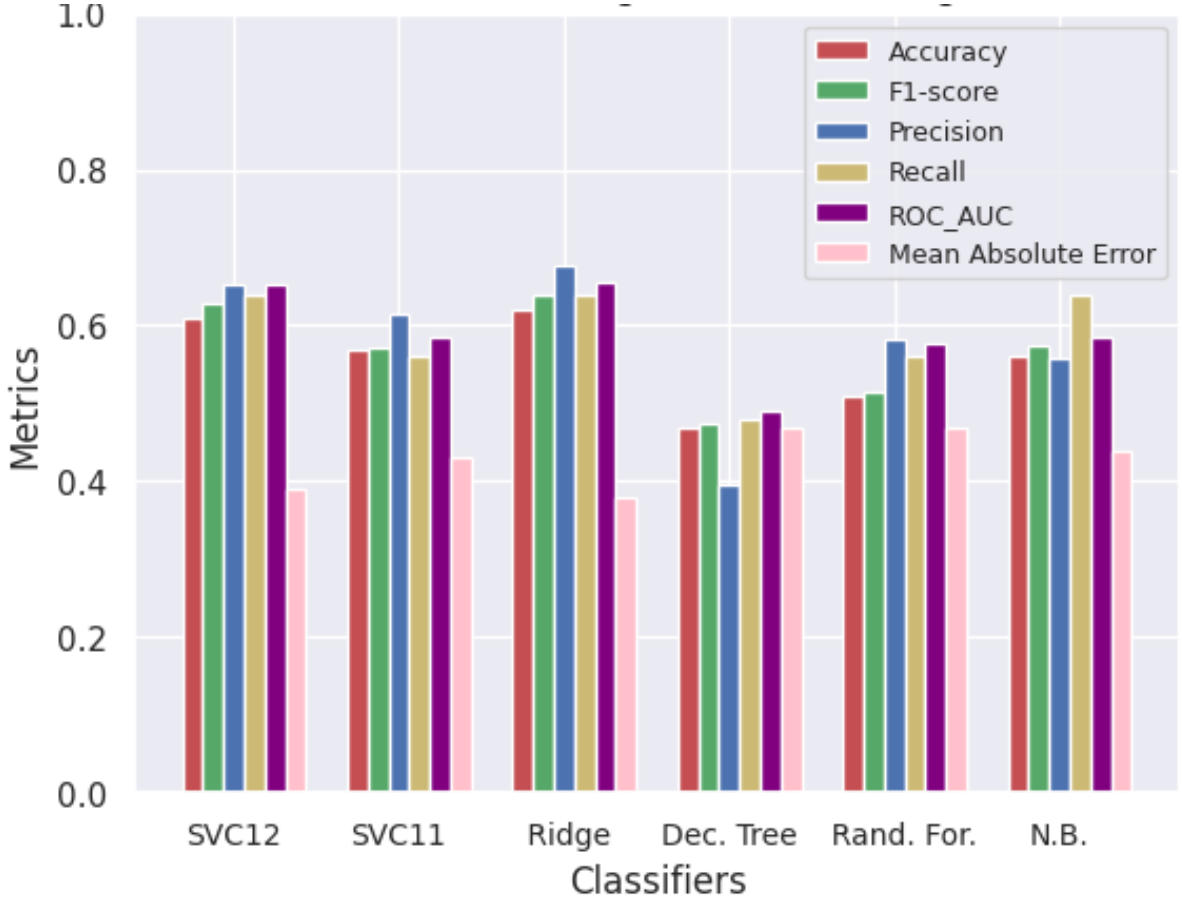

Figure 4.13 Performance comparison of six ML classifiers using AAL atlas

In the case of AAL atlas, six machine learning classifiers have a peak of the median ROC_AUC value varied from 0.47 to 0.65 and an accuracy of around 0.6. Top performing model is Ridge Classifier with all evaluation metrics outperform other classifiers and having an accuracy of 64%, precision of 68%, sensitivity of 64% and ROC_AUC value of 66%.

Table 4.3 Performance results using Harvard-Oxford atlas

	SVC L2	SVC L1	Ridge Classifier	Decision Tree	Random Forest	Naïve Bayes
Accuracy	0.640	**0.660**	0.650	0.540	0.420	0.550
F1-score	0.618	**0.643**	0.630	0.539	0.552	0.529
Precision	0.583	**0.697**	0.600	0.564	0.531	0.568
Recall	0.680	**0.700**	0.680	0.600	0.420	0.540
ROC_AUC	0.624	**0.724**	0.628	0.538	0.492	0.584
MAE	0.370	**0.340**	0.350	0.440	0.400	0.450

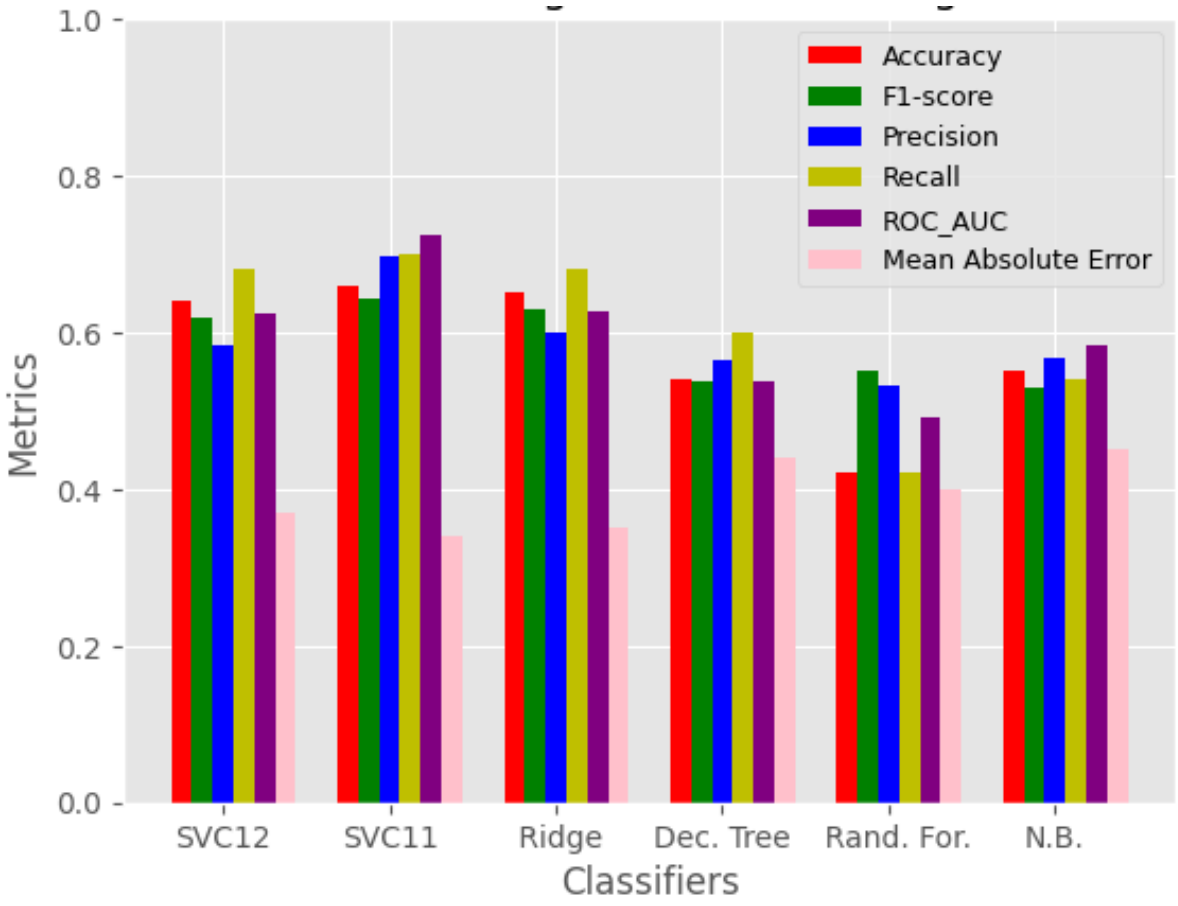

Figure 4.14 Performance comparison of six ML classifiers using H-O atlas

ASD detection performance results of six machine learning classifiers are presented in Table 4.3. As illustrated in Figure 4.14, it is apparent that parse (*l1*) Support Vector Classifier has the best results when using Harvard-Oxford atlas with accuracy, precision, sensitivity and AUC score of 66%, 70%, 70% and 72%, respectively.

Table 4.4 Performance results using Juelich atlas

	SVC L2	SVC L1	Ridge Classifier	Decision Tree	Random Forest	Naïve Bayes
Accuracy	**0.690**	0.580	0.660	0.639	0.520	0.530
F1-score	**0.658**	0.607	0.653	0.641	0.499	0.505
Precision	**0.690**	0.606	0.658	0.639	0.535	0.515
Recall	**0.701**	0.666	0.715	0.700	0.654	0.546
ROC_AUC	**0.844**	0.719	0.840	0.655	0.627	0.573
MAE	**0.330**	0.400	0.339	0.400	0.550	0.470

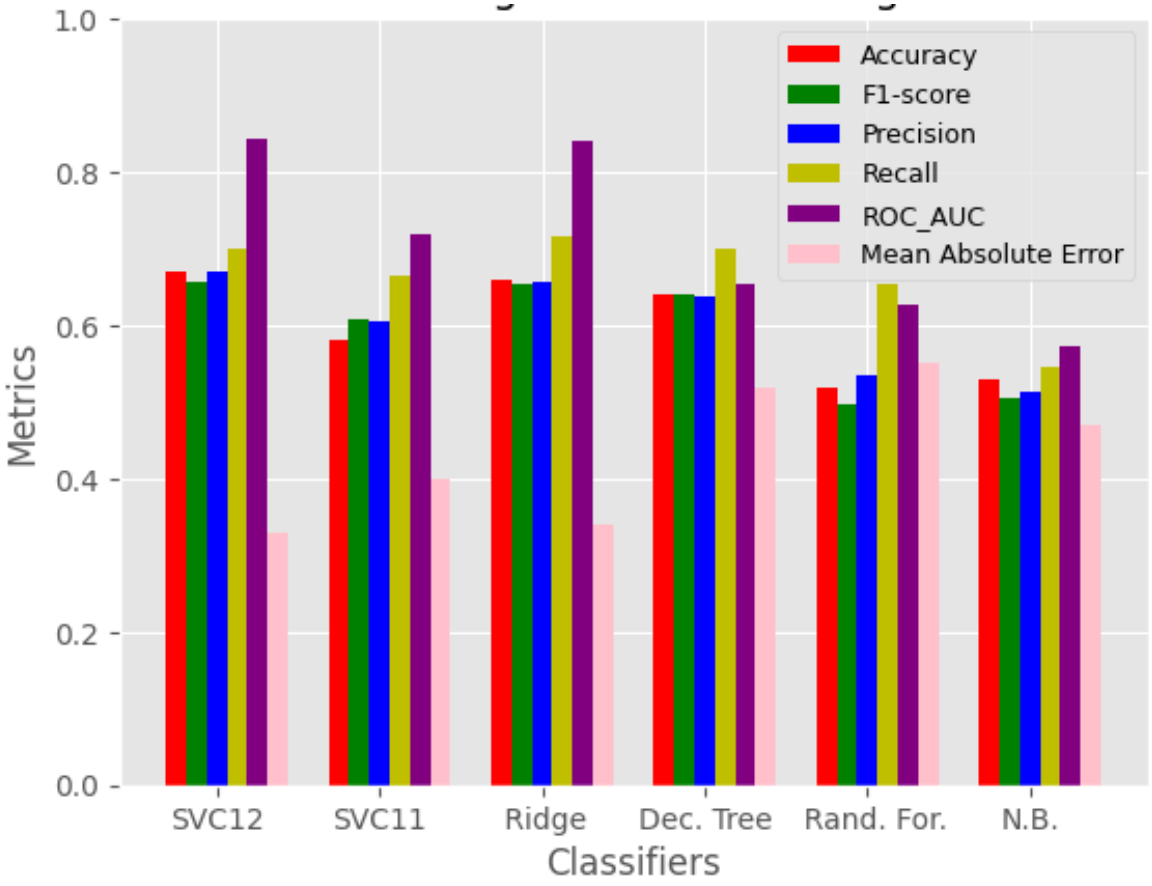

Figure 4.15 Performance comparison of six ML classifiers using Juelich atlas

Peformance results of classifying ASD and TC subjects using Juelich atlas achieved the top performing outcome with non-parse (*l2*) Support Vector Classifier, which are 69.0% accuracy, 69.0% precision, 70.1% recall and 84% AUC-ROC.

4.3.3. General Remarks

From Table 4.2, 4.3 and 4.4, we can also easily observe that among three kinds of brain atlas, Juelich is the most promising atlas to detect ASD from rs-fMRI for the future study with the evaluation metrics improve over all other brain atlases. The best result has an accuracy of 69%, precision of 69%, sensitivity of 70% and AUC of 84%. This conclusion also confirms that parcellation containing a larger number of ROIs can represent functional connectivity patterns at the voxel level and more accurate.

In addition, as we can see from the tables and figures above about the effects of brain parcellations and classifiers choices on classifying ASD and TC subject, apparently, all the presented median ROC-AUC values have a peak around the value 0.6, which is near equivalent to random choice. This is a clear indication of the difficulty of the problem. Most pipeline combinations are not good performers and results are quite unstable in general, with big variations between cross validation repetitions. Hence, this is the most salient empirical demonstration of the data heterogeneity and the need for careful design of large scale data collection efforts. Data heterogeneity is due to site differences on data capture devices and procedures, as well as implementation of diagnostic criteria. Another source of heterogeneity is the openess of the diagnostic criteria leading to the inclussion of subjects with widely diverse cognitive signatures.

4.4. Deep Learning-based Results using LSTM

4.4.1. Training Settings

For classification of ASD and TC subjects from rs-fMRI data using LSTM-based model, the dataset was divided into three parts, a training set, a validation set, and a test set. Initially, the data is split 80 percent into a training set and the remaining 20 percent into a test set. Then the 20% data from the training set is used for the

validation set. The hyperparameters for the LSTM and GRU model are the batch sizes, the learning rate, the optimizers, and the number of epochs. The epochs of 100 were chosen and the model used was applied the early stopping criterion from the Keras library; the model will stop training if there is no improvement in the validation loss five consecutive times. Since the value of epochs is allowed to be sufficiently high, the early stopping criterion chooses the appropriate value of epochs. During the training, we fixed the training epoch to 100. The remaining hyperparameters were chosen using hyperparameter tuning. The choice of the optimizers was Adam. The learning rate was chosen the value of 0.001. The batch size of 32 were considered and the binary cross-entropy was used as loss function.

4.4.2. Experimental Results

In this work, we have proposed an LTSM model with Dropout layer to detect ASD showing different measurement metrics in the same manner with accuracy, precision and sensitivity or recall to legitimize the performance of the proposed method. The model training accuracy and loss curves are presented in Fig. 4.16. From Figure 4.16, it is depicting that the training accuracy is increasing with decreasing the training loss.

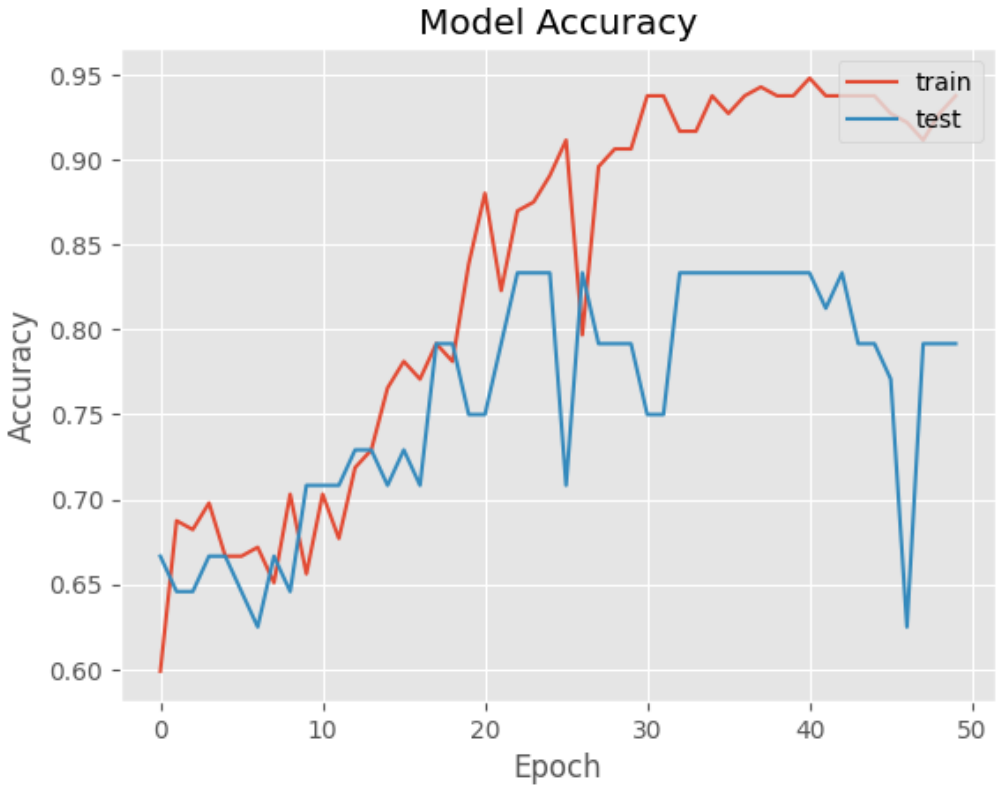

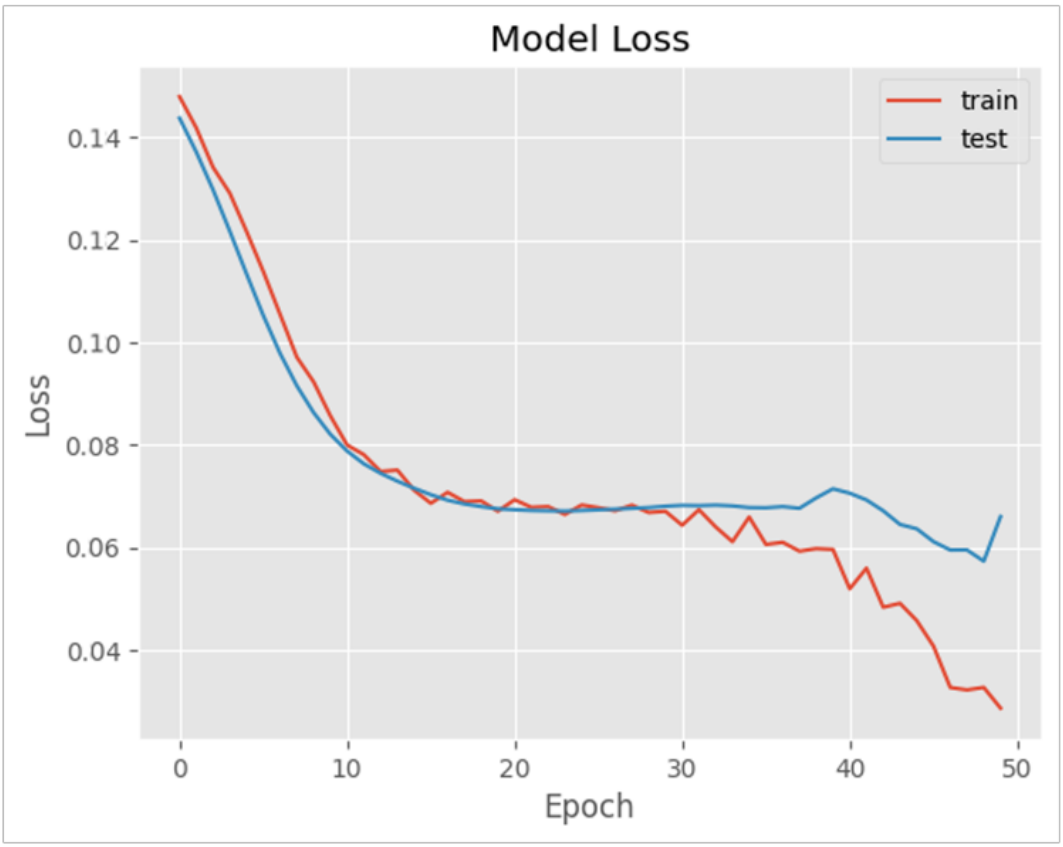

Figure 4.16 Accuracy and loss depending on the number of epoch for LSTM model

With the above mentioned parameters, the proposed LSTM model with Dropout layers achieved a best autism detection accuracy of 78.24% with Juelich atlas. Table 4.4 shows the performance values for different brain atlases including accuracy, precision and sensitivity for ASD classification using proposed LSTM-based model. After testing our model for ASD classification, this thesis achieved the highest accuracy of 78.24% with Juelich atlas, the precision of 72.56% with AAL atlas and sensitivity of 76.96% with Juelich atlas. Table 4.5 shows the detailed performance evaluation metrics using proposed LSTM model with three different brain atlases.

Table 4.5 Performance results using Juelich atlas

Metrics	AAL	HO	Juelich
Accuracy	73.87%	72.64%	**78.24%**
Precision	**72.56%**	69.85%	71.73%
Sensitivity	69.93%	74.57%	**76.96%**

In comparison with the results using conventional machine learning methods (refer to Table 4.2, 4.3, 4.4 for results obtained using different conventional machine learning methods), the deep learning approach using LSTM-based model gained around 10% in performance metrics for ASD detection.

4.5. Comparison with Other Works

The experimental results tested and verified the effectiveness of the research method of classifying ASD and TC from rs-fMRI using machine learning and deep learning. This thesis have achieved the highest accuracy of 78.24% with LSTM-based model on the whole ABIDE I cohort. Table 4.5 compares the best result of this research with other works.

Table 4.6 Comparing the best result of this research with other works

Methods	Accuracy (%)
Abraham et al. [71]	66.80
Eslami et al. [117]	70.10
Mostafa et al. [118]	77.70
Parisot et al. [119]	69.50
Xin Yang et al. [120]	71.98
This thesis	**78.24**

CHAPTER 5. CONCLUSION AND FUTURE WORK

5.1. Conclusion

ASD is a group of heterogeneous developmental disabilities that developed in early childhood. However, the diagnosis of ASD is mainly depend on the behavioral assessment which is subjective, time consuming and not reliable. ASD detection is a challenging task since no standard modeling choice has yet been recognized, and the current practice is very much diverse. Hence, finding an objective and reliable diagnostic method for ASD is imperative and deep in meaning.

The work of this thesis analyzed rs-fMRI brain image data obtained from Preprocessed ABIDE dataset combined with machine learning and deep learning techniques to diagnose ASD from TD. First of all, to extract mean BOLD signals from preprocessed data, brain atlases were used. A single brain atlas that can serve as a biomarker for the detection of ASD has not yet been discovered. Thus, three different standard and predefined atlases were used to extract ROIs. Then, connectivity matrices were prepared using tangent embedding and flattened to form a feature vector removing redundant information. After performing a wide array of experiments, it has been confirmed that the Juelich atlas using 121 ROIs yields higher predictive power than AAL and Harvard-Oxford atlases and can be considered to be more reliable in ASD diagnosis. It achieved 69% accuracy, 66% F1-score and 84% ROC-AUC. In addition, a deep learning-based method using LSTM model with Dropout layer was also implemented with an accuracy of 78.24%. This result transcends most of the performances of existing works indicating that it is a promising method for ASD diagnosis. The successful implementation of this method may be used for a wide range of applications, such as identifying neural activation patterns responsible for autism and performing visual evaluation of the functional characteristics of the autistic brain. Besides, by examining the contrast between the autistic and control brain, the underlying neural or biological basis of ASD is also unveiled and established.

5.2. Future Work

Based on the studies conducted in this thesis, several future directions for the classification task of individuals with ASD and TD are proposed. Future work should address the extension of the computational experiments to the full extent of the ABIDE II dataset. Other conectomics datasets collecting subjects and controls from connectivity analysis regarding other diseases will also be considered. In addition, a novel attention algorithm may be developed to improve the performance of deep learning models. Attention mechanism has revolutionized the fields like Natural Language Processing (NLP) and computer vision (CV). The basic idea behind attention mechanism is to focus on specific parts of the input, rather than all available information. Future work will also explore the relevance of diagnostic criteria implementation and the data capture differences among sites to provide more robust performance predictions leading to better grounded biomarker identification.

REFERENCES

[1] S. Bhat, U. R. Acharya, H. Adeli, G. M. Bairy, and A. Adeli, "Autism: Cause factors, early diagnosis and therapies," *Reviews in the Neurosciences*, vol. 25, no. 6, 2014. doi:10.1515/revneuro-2014-0056

[2] "Correction and republication: Prevalence and characteristics of autism spectrum disorder among children aged 8 years — autism and Developmental Disabilities Monitoring Network, 11 sites, United States, 2012," MMWR. *Morbidity and Mortality Weekly Repor*t, vol. 67, no. 45, p. 1279, 2018. doi:10.15585/mmwr.mm6745a7

[3] V. Hus and C. Lord, "The Autism Diagnostic Observation Schedule, module 4: Revised algorithm and standardized severity scores," *Journal of Autism and Developmental Disorders*, vol. 44, no. 8, pp. 1996–2012, 2014. doi:10.1007/s10803-014-2080-3

[4] C. Lord, M. Rutter, and A. Le Couteur, "Autism diagnostic interview-revised: A revised version of a diagnostic interview for caregivers of individuals with possible pervasive developmental disorders," *Journal of Autism and Developmental Disorders*, vol. 24, no. 5, pp. 659–685, 1994. doi:10.1007/bf02172145

[5] E. Varol, B. Gaonkar, G. Erus, R. Schultz, and C. Davatzikos, "Feature ranking based nested support Vector Machine Ensemble for Medical Image Classification," *2012 9th IEEE International Symposium on Biomedical Imaging (ISBI)*, 2012. doi:10.1109/isbi.2012.6235505

[6] N. C. Dvornek, P. Ventola, and J. S. Duncan, "Combining phenotypic and resting-state fmri data for Autism Classification with Recurrent Neural Networks," *2018 IEEE 15th International Symposium on Biomedical Imaging (ISBI 2018)*, 2018. doi:10.1109/isbi.2018.8363676

[7] O. Altay and M. Ulas, "Prediction of the autism spectrum disorder diagnosis with linear discriminant analysis classifier and K-nearest neighbor in children," *2018 6th International Symposium on Digital Forensic and Security (ISDFS)*, 2018. doi:10.1109/isdfs.2018.8355354

[8] T. Vos et al., "Global, regional, and national incidence, prevalence, and years lived with disability for 310 diseases and injuries, 1990–2015: a systematic

analysis for the Global Burden of Disease Study 2015," *The Lancet*, vol. 388, no. 10053, pp. 1545–1602, Oct. 2016, doi: 10.1016/s0140-6736(16)31678-6

[9] Autism Speaks Canada, "About autism - Autism Speaks Canada," *Autism Speaks Canada*, May 26, 2023. https://www.autismspeaks.ca/about/about-autism

[10] J. Baio et al., "Prevalence of autism spectrum disorder among children aged 8 years — Autism and Developmental Disabilities Monitoring Network, 11 sites, United States, 2014," *Morbidity and Mortality Weekly Report*, vol. 67, no. 6, pp. 1–23, Apr. 2018, doi: 10.15585/mmwr.ss6706a1

[11] C. J. Newschaffer et al., "The Epidemiology of autism spectrum Disorders," *Annual Review of Public Health*, vol. 28, no. 1, pp. 235–258, Apr. 2007, doi: 10.1146/annurev.publhealth.28.021406.144007

[12] "Diagnostic and Statistical Manual of Mental Disorders: DSM-5 (5th edition)," *Reference Reviews*, vol. 28, no. 3, pp. 36–37, Mar. 2014, doi: 10.1108/rr-10-2013-0256

[13] L. Kanner, "Autistic disturbances of affective contact," *The Nervous Child*, vol. 2, pp. 217–250, Jan. 1943, [Online]. Available: http://ci.nii.ac.jp/naid/10018378330

[14] H. Asperger, "Die „Autistischen Psychopathen" im Kindesalter," *Archiv Für Psychiatrie Und Nervenkrankheiten*, vol. 117, no. 1, pp. 76–136, Jun. 1944, doi: 10.1007/bf01837709

[15] L. Wing and J. Gould, "Severe impairments of social interaction and associated abnormalities in children: Epidemiology and classification," *Journal of Autism and Developmental Disorders*, vol. 9, no. 1, pp. 11–29, Mar. 1979, doi: 10.1007/bf01531288

[16] A. Bailey et al., "Autism as a strongly genetic disorder: evidence from a British twin study," *Psychological Medicine*, vol. 25, no. 1, pp. 63–77, Jan. 1995, doi: 10.1017/s0033291700028099

[17] "Autism spectrum Disorder," *National Institute of Mental Health (NIMH)*. https://www.nimh.nih.gov/health/topics/autism-spectrum-disorders-asd/index.shtml

[18] R. Lenroot and P. K. Yeung, “Heterogeneity within Autism Spectrum Disorders: What have We Learned from Neuroimaging Studies?,” *Frontiers in Human Neuroscience*, vol. 7, Jan. 2013, doi: 10.3389/fnhum.2013.00733

[19] B. Zablotsky, L. I. Black, M. J. Maenner, L. A. Schieve, and S. J. Blumberg, “Estimated prevalence of autism and other developmental disabilities following questionnaire changes in the 2014 National Health Interview Survey.,” *PubMed*, no. 87, pp. 1–20, Nov. 2015, [Online]. Available: https://pubmed.ncbi.nlm.nih.gov/26632847

[20] S. Bhat, U. R. Acharya, H. Adeli, G. M. Bairy, and A. Adeli, “Automated diagnosis of autism: in search of a mathematical marker,” *Reviews in the Neurosciences*, vol. 25, no. 6, Jan. 2014, doi: 10.1515/revneuro-2014-0036

[21] H. Noğay and H. Adeli, “Machine learning (ML) for the diagnosis of autism spectrum disorder (ASD) using brain imaging,” *Reviews in the Neurosciences*, vol. 31, no. 8, pp. 825–841, Aug. 2020, doi: 10.1515/revneuro-2020-0043

[22] F. Segovia et al., “Identifying endophenotypes of autism: a multivariate approach,” *Frontiers in Computational Neuroscience*, vol. 8, Jun. 2014, doi: 10.3389/fncom.2014.00060

[23] L. Q. Uddin, D. R. Dajani, W. Voorhies, H. M. Bednarz, and R. K. Kana, “Progress and roadblocks in the search for brain-based biomarkers of autism and attention-deficit/hyperactivity disorder,” *Translational Psychiatry*, vol. 7, no. 8, p. e1218, Aug. 2017, doi: 10.1038/tp.2017.164.

[24] J. Granich et al., “Randomised controlled trial of an iPad based early intervention for autism: TOBY playpad study protocol,” *BMC Pediatrics*, vol. 16, no. 1, Oct. 2016, doi: 10.1186/s12887-016-0704-9

[25] E. Cravedi et al., “Disentangling Tourette syndrome heterogeneity through hierarchical ascendant clustering,” *Developmental Medicine & Child Neurology*, vol. 60, no. 9, pp. 942–950, May 2018, doi: 10.1111/dmcn.13913

[26] H. De Jaegher, “Embodiment and sense-making in autism,” *Frontiers in Integrative Neuroscience*, vol. 7, 2013. doi:10.3389/fnint.2013.00015

[27] M. D. Kaiser and K. A. Pelphrey, “Disrupted action perception in autism: Behavioral evidence, neuroendophenotypes, and diagnostic utility,” *Developmental Cognitive Neuroscience*, vol. 2, no. 1, pp. 25–35, 2012. doi:10.1016/j.dcn.2011.05.005

[28] M. Turi, F. Muratori, F. Tinelli, M. C. Morrone, and D. C. Burr, “Autism is associated with reduced ability to interpret grasping actions of others,” *Scientific Reports*, vol. 7, no. 1, 2017. doi:10.1038/s41598-017-12995-z

[29] B. Li, A. Sharma, J. Meng, S. Purushwalkam, and E. Gowen, “Applying machine learning to identify autistic adults using imitation: An exploratory study,” *PLOS ONE*, vol. 12, no. 8, 2017. doi:10.1371/journal.pone.0182652

[30] A. Anzulewicz, K. Sobota, and J. T. Delafield-Butt, “Toward the autism motor signature: Gesture patterns during smart tablet gameplay identify children with autism,” *Scientific Reports*, vol. 6, no. 1, 2016. doi:10.1038/srep31107

[31] A. V. Maharaj, A. Gutierrez, C. Cueto, and S. Cadavid, “Automated measurement of repetitive behavior using the Microsoft kinect: A proof of concept,” *Behavioral Interventions*, vol. 35, no. 4, pp. 488–497, 2020. doi:10.1002/bin.1746

[32] V. Focaroli, F. Taffoni, S. M. Parsons, F. Keller, and J. M. Iverson, “Performance of motor sequences in children at heightened vs. low risk for ASD: A longitudinal study from 18 to 36 months of age,” *Frontiers in Psychology*, vol. 7, 2016. doi:10.3389/fpsyg.2016.00724

[33] B. Ge, H. W. Park, and A. M. Howard, “Identifying Engagement from Joint Kinematics Data for Robot Therapy Prompt Interventions for Children with Autism Spectrum Disorder,” in *Lecture Notes in Computer Science*, 2016, pp. 531–540. doi: 10.1007/978-3-319-47437-3_52

[34] I. B. Wijayasinghe, I. Ranatunga, N. Balakrishnan, N. L. Bugnariu, and D. O. Popa, “Human–Robot Gesture Analysis for Objective Assessment of autism Spectrum Disorder,” *International Journal of Social Robotics*, vol. 8, no. 5, pp. 695–707, Oct. 2016, doi: 10.1007/s12369-016-0379-2

[35] K. S. Lohan, E. Sheppard, G. Little and G. Rajendran, "Toward Improved Child–Robot Interaction by Understanding Eye Movements," in *IEEE Transactions on Cognitive and Developmental Systems*, vol. 10, no. 4, pp. 983-992, Dec. 2018, doi: 10.1109/TCDS.2018.2838342.

[36] A. Banerjee, M. Pal, S. Datta, D. N. Tibarewala, and A. Konar, “Eye movement sequence analysis using electrooculogram to assist autistic children,” *Biomedical Signal Processing and Control*, vol. 14, pp. 134–140, Nov. 2014, doi: 10.1016/j.bspc.2014.07.010

[37] T. Kujala, S. Kuuluvainen, S. Saalasti, E. Jansson-Verkasalo, L. Von Wendt, and T. Lepistö, “Speech-feature discrimination in children with Asperger syndrome as determined with the multi-feature mismatch negativity paradigm,” *Clinical Neurophysiology*, vol. 121, no. 9, pp. 1410–1419, Sep. 2010, doi: 10.1016/j.clinph.2010.03.017

[38] P. Stribling, J. Rae, and P. Dickerson, “Using conversation analysis to explore the recurrence of a topic in the talk of a boy with an autism spectrum disorder,” *Clinical Linguistics & Phonetics*, vol. 23, no. 8, pp. 555–582, Jan. 2009, doi: 10.1080/02699200802491165

[39] A. Haffey, C. Press, G. O’Connell, and B. Chakrabarti, “Autistic Traits Modulate Mimicry of Social but not Nonsocial Rewards,” *Autism Research*, vol. 6, no. 6, pp. 614–620, Aug. 2013, doi: 10.1002/aur.1323

[40] S. Bhat, U. R. Acharya, H. Adeli, G. M. Bairy, and A. Adeli, “Automated diagnosis of autism: in search of a mathematical marker,” *Reviews in the Neurosciences*, vol. 25, no. 6, Jan. 2014, doi: 10.1515/revneuro-2014-0036

[41] R. Djemal, K. AlSharabi, S. Ibrahim, and A. Alsuwailem, “EEG-based computer aided diagnosis of autism spectrum disorder using wavelet, entropy, and ann,” *BioMed Research International*, vol. 2017, pp. 1–9, 2017. doi:10.1155/2017/9816591

[42] E. Grossi, C. Olivieri, and M. Buscema, “Diagnosis of autism through EEG processed by Advanced Computational Algorithms: A pilot study,” *Computer Methods and Programs in Biomedicine*, vol. 142, pp. 73–79, 2017. doi:10.1016/j.cmpb.2017.02.002

[43] B. A. Cociu et al., “Multimodal Functional and Structural brain connectivity analysis in Autism: a preliminary integrated approach with EEG, FMRI, and DTI,” *IEEE Transactions on Cognitive and Developmental Systems*, vol. 10, no. 2, pp. 213–226, Jun. 2018, doi: 10.1109/tcds.2017.2680408.

[44] S. Ha, I. J. Sohn, N. Kim, H. J. Sim, and K.-A. Cheon, “Characteristics of Brains in Autism Spectrum Disorder: Structure, Function and Connectivity across the Lifespan,” *Experimental Neurobiology*, vol. 24, no. 4, pp. 273–284, Dec. 2015, doi: 10.5607/en.2015.24.4.273

[45] M. Schuetze, M. T. M. Park, I. Y. Cho, F. P. MacMaster, M. M. Chakravarty, and S. Bray, “Morphological alterations in the thalamus, striatum, and pallidum in

autism spectrum disorder," *Neuropsychopharmacology*, vol. 41, no. 11, pp. 2627–2637, Apr. 2016, doi: 10.1038/npp.2016.64

[46] E. Conti et al., "Network over-connectivity differentiates autism spectrum disorder from other developmental disorders in toddlers: A diffusion MRI study," *Human Brain Mapping*, vol. 38, no. 5, pp. 2333–2344, Jan. 2017, doi: 10.1002/hbm.23520

[47] J. Wang, Q. Wang, H. Zhang, J. Chen, S. Wang, and D. Shen, "Sparse multiview Task-Centralized ensemble learning for ASD diagnosis based on age- and Sex-Related functional connectivity patterns," *IEEE Transactions on Cybernetics*, vol. 49, no. 8, pp. 3141–3154, Aug. 2019, doi: 10.1109/tcyb.2018.2839693

[48] G. Chanel, S. Pichon, L. Conty, S. Berthoz, C. Chevallier, and J. Grèzes, "Classification of autistic individuals and controls using cross-task characterization of fMRI activity," *NeuroImage: Clinical*, vol. 10, pp. 78–88, Jan. 2016, doi: 10.1016/j.nicl.2015.11.010

[49] L. E. Libero, T. P. DeRamus, A. C. Lahti, G. Deshpande, and R. K. Kana, "Multimodal neuroimaging based classification of autism spectrum disorder using anatomical, neurochemical, and white matter correlates," *Cortex*, vol. 66, pp. 46–59, May 2015, doi: 10.1016/j.cortex.2015.02.008

[50] C. P. Chen et al., "Diagnostic classification of intrinsic functional connectivity highlights somatosensory, default mode, and visual regions in autism," *NeuroImage: Clinical*, vol. 8, pp. 238–245, Jan. 2015, doi: 10.1016/j.nicl.2015.04.002

[51] X. Guo, K. C. Dominick, A. A. Minai, H. Li, C. A. Erickson, and L. Lu, "Diagnosing Autism Spectrum Disorder from Brain Resting-State Functional Connectivity Patterns Using a Deep Neural Network with a Novel Feature Selection Method," *Frontiers in Neuroscience*, vol. 11, Aug. 2017, doi: 10.3389/fnins.2017.00460

[52] B. Sen, N. C. Borle, R. Greiner, and M. Brown, "A general prediction model for the detection of ADHD and Autism using structural and functional MRI," *PLOS ONE*, vol. 13, no. 4, p. e0194856, Apr. 2018, doi: 10.1371/journal.pone.0194856

[53] A. S. Nunes, N. Peatfield, V. A. Vakorin, and S. M. Doesburg, "Idiosyncratic organization of cortical networks in autism spectrum disorder," *NeuroImage*, vol. 190, pp. 182–190, Apr. 2019, doi: 10.1016/j.neuroimage.2018.01.022

[54] C. Y. Wee, P. T. Yap, and D. Shen, “Diagnosis of autism spectrum disorders using temporally distinct Resting-State functional connectivity networks,” *CNS Neuroscience & Therapeutics*, vol. 22, no. 3, pp. 212–219, Jan. 2016, doi: 10.1111/cns.12499

[55] X. Xiao et al., “Diagnostic model generated by MRI-derived brain features in toddlers with autism spectrum disorder,” *Autism Research*, vol. 10, no. 4, pp. 620–630, Nov. 2016, doi: 10.1002/aur.1711

[56] J. T. O’Brien, “Role of imaging techniques in the diagnosis of dementia,” *British Journal of Radiology*, vol. 80, no. special_issue_2, pp. S71–S77, Dec. 2007, doi: 10.1259/bjr/33117326

[57] C. S. Carter and J. W. Dalley, Brain imaging in behavioral neuroscience. *Springer Science & Business Media*, 2011

[58] Y. Assaf and O. Pasternak, “Diffusion Tensor Imaging (DTI)-based white matter Mapping in Brain Research: A review,” *Journal of Molecular Neuroscience*, vol. 34, no. 1, pp. 51–61, Sep. 2007, doi: 10.1007/s12031-007-0029-0

[59] M. E. Raichle, “Behind the scenes of functional brain imaging: A historical and physiological perspective,” *Proceedings of the National Academy of Sciences of the United States of America*, vol. 95, no. 3, pp. 765–772, Feb. 1998, doi: 10.1073/pnas.95.3.765

[60] T. F. Massoud and S. S. Gambhir, “Molecular imaging in living subjects: seeing fundamental biological processes in a new light,” *Genes & Development*, vol. 17, no. 5, pp. 545–580, Mar. 2003, doi: 10.1101/gad.1047403

[61] A. M. Michael et al., “A Data-Driven Investigation of Gray Matter–Function Correlations in Schizophrenia during a Working Memory Task,” *Frontiers in Human Neuroscience*, vol. 5, Jan. 2011, doi: 10.3389/fnhum.2011.00071

[62] R. W. Brown, N. Cheng, E. M. Haacke, M. R. Thompson, and R. Venkatesan, *Magnetic resonance imaging: Physical Principles and Sequence Design*. John Wiley & Sons, 2014

[63] S. Ogawa, T. M. Lee, A. R. Kay, and D. W. Tank, “Brain magnetic resonance imaging with contrast dependent on blood oxygenation.,” *Proceedings of the National Academy of Sciences of the United States of America*, vol. 87, no. 24, pp. 9868–9872, Dec. 1990, doi: 10.1073/pnas.87.24.9868

[64] P. C. Lauterbur, “Image formation by induced local interactions: Examples employing nuclear magnetic resonance,” *Nature*, vol. 242, no. 5394, pp. 190–191, Mar. 1973, doi: 10.1038/242190a0

[65] A. C. Evans, D. L. Collins, S. Mills, E. D. Brown, R. Kelly, and T. M. Peters, “3D statistical neuroanatomical models from 305 MRI volumes,” *IEEE*, Aug. 2005, doi: 10.1109/nssmic.1993.373602

[66] A. D. C. Van Essen et al., “The Human Connectome Project: A data acquisition perspective,” *NeuroImage*, vol. 62, no. 4, pp. 2222–2231, Oct. 2012, doi: 10.1016/j.neuroimage.2012.02.018.

[67] C. Sudlow et al., “UK Biobank: an open access resource for identifying the causes of a wide range of complex diseases of middle and old age,” *PLOS Medicine*, vol. 12, no. 3, p. e1001779, Mar. 2015, doi: 10.1371/journal.pmed.1001779

[68] M. D. Greicius, “Resting-state functional connectivity in neuropsychiatric disorders,” *Current Opinion in Neurology*, vol. 21, no. 4, pp. 424–430, Aug. 2008, doi: 10.1097/wco.0b013e328306f2c5

[69] C. O’Callaghan, M. Hornberger, J. H. Balsters, G. M. Halliday, S. J. G. Lewis, and J. M. Shine, “Cerebellar atrophy in Parkinson’s disease and its implication for network connectivity,” *Brain*, vol. 139, no. 3, pp. 845–855, Jan. 2016, doi: 10.1093/brain/awv399

[70] A. Alexandre et al., “Deriving reproducible biomarkers from multi-site resting-state data: An Autism-based example,” *NeuroImage*, vol. 147, pp. 736–745, Feb. 2017, doi: 10.1016/j.neuroimage.2016.10.045

[71] Y.-F. Zang et al., “Altered baseline brain activity in children with ADHD revealed by resting-state functional MRI,” *Brain & Development*, vol. 29, no. 2, pp. 83–91, Mar. 2007, doi: 10.1016/j.braindev.2006.07.002

[72] S. M. Smith et al., “A positive-negative mode of population covariation links brain connectivity, demographics and behavior,” *Nature Neuroscience*, vol. 18, no. 11, pp. 1565–1567, Sep. 2015, doi: 10.1038/nn.4125

[73] M. Fox and M. E. Raichle, “Spontaneous fluctuations in brain activity observed with functional magnetic resonance imaging,” *Nature Reviews Neuroscience*, vol. 8, no. 9, pp. 700–711, Sep. 2007, doi: 10.1038/nrn2201

[74] M. Rahim, B. Thirion, and G. Varoquaux, “Population-Shrinkage of covariance to estimate better brain functional connectivity,” in *Springer eBooks*, 2017, pp. 460–468. doi: 10.1007/978-3-319-66182-7_53

[75] M. R. Sabuncu, B. D. Singer, B. Conroy, R. E. Bryan, P. J. Ramadge, and J. V. Haxby, “Function-based intersubject alignment of human cortical anatomy,” *Cerebral Cortex*, vol. 20, no. 1, pp. 130–140, May 2009, doi: 10.1093/cercor/bhp085

[76] M. D. Greicius, B. Krasnow, A. L. Reiss, and V. Menon, “Functional connectivity in the resting brain: A network analysis of the default mode hypothesis,” *Proceedings of the National Academy of Sciences of the United States of America*, vol. 100, no. 1, pp. 253–258, Dec. 2002, doi: 10.1073/pnas.0135058100

[77] A. K. Roy et al., “Functional connectivity of the human amygdala using resting state fMRI,” *NeuroImage*, vol. 45, no. 2, pp. 614–626, Apr. 2009, doi: 10.1016/j.neuroimage.2008.11.030

[78] S. C. Strother, “Evaluating fMRI preprocessing pipelines,” *IEEE Engineering in Medicine and Biology Magazine*, vol. 25, no. 2, pp. 27–41, Mar. 2006, doi: 10.1109/memb.2006.1607667

[79] A. Di Martino et al., “The autism brain imaging data exchange: towards a large-scale evaluation of the intrinsic brain architecture in autism,” *Molecular Psychiatry*, vol. 19, no. 6, pp. 659–667, Jun. 2013, doi: 10.1038/mp.2013.78

[80] “ABIDE preprocessed.” http://preprocessed-connectomes-project.org/abide

[81] K. Amunts and K. Zilles, “Architectonic Mapping of the Human Brain beyond Brodmann,” *Neuron*, vol. 88, no. 6, pp. 1086–1107, Dec. 2015, doi: 10.1016/j.neuron.2015.12.001

[82] N. U. F. Dosenbach et al., “Prediction of individual brain maturity using FMRI,” *Science*, vol. 329, no. 5997, pp. 1358–1361, Sep. 2010, doi: 10.1126/science.1194144

[83] A. Alexandre et al., “Deriving reproducible biomarkers from multi-site resting-state data: An Autism-based example,” *NeuroImage*, vol. 147, pp. 736–745, Feb. 2017, doi: 10.1016/j.neuroimage.2016.10.045

[84] S. Arslan, S. I. Ktena, A. Makropoulos, E. C. Robinson, D. Rueckert, and S. Parisot, “Human brain mapping: A systematic comparison of parcellation

methods for the human cerebral cortex," *NeuroImage*, vol. 170, pp. 5–30, Apr. 2018, doi: 10.1016/j.neuroimage.2017.04.014

[85] K. Dadi et al., "Benchmarking functional connectome-based predictive models for resting-state fMRI," *NeuroImage*, vol. 192, pp. 115–134, May 2019, doi: 10.1016/j.neuroimage.2019.02.062

[86] S. B. Eickhoff et al., "Assignment of functional activations to probabilistic cytoarchitectonic areas revisited," *NeuroImage*, vol. 36, no. 3, pp. 511–521, Jul. 2007, doi: 10.1016/j.neuroimage.2007.03.060

[87] R. S. Desikan et al., "An automated labeling system for subdividing the human cerebral cortex on MRI scans into gyral based regions of interest," *NeuroImage*, vol. 31, no. 3, pp. 968–980, Jul. 2006, doi: 10.1016/j.neuroimage.2006.01.021

[88] E. T. Rolls, C.-C. Huang, C. P. Lin, J. Feng, and M. Joliot, "Automated anatomical labelling atlas 3," *NeuroImage*, vol. 206, p. 116189, Feb. 2020, doi: 10.1016/j.neuroimage.2019.116189

[89] R. C. Craddock, G. A. James, P. E. Holtzheimer, X. Hu, and H. S. Mayberg, "A whole brain fMRI atlas generated via spatially constrained spectral clustering.," *Human Brain Mapping*, Aug. 2012, doi: 10.1002/hbm.21333

[90] K. Amunts, H. Mohlberg, S. Bludau, and K. Zilles, "Julich-Brain: A 3D probabilistic atlas of the human brain's cytoarchitecture," *Science*, vol. 369, no. 6506, pp. 988–992, Jul. 2020, doi: 10.1126/science.abb4588

[91] K. J. Friston, P. Jezzard, and R. Turner, "Analysis of functional MRI time-series," *Human Brain Mapping*, vol. 1, no. 2, pp. 153–171, Jan. 1994, doi: 10.1002/hbm.460010207

[92] M. D. Greicius, B. Krasnow, A. L. Reiss, and V. Menon, "Functional connectivity in the resting brain: A network analysis of the default mode hypothesis," *Proceedings of the National Academy of Sciences of the United States of America*, vol. 100, no. 1, pp. 253–258, Dec. 2002, doi: 10.1073/pnas.0135058100

[93] O. Ledoit and M. Wolf, "A well-conditioned estimator for large-dimensional covariance matrices," *Journal of Multivariate Analysis*, vol. 88, no. 2, pp. 365–411, Feb. 2004, doi: 10.1016/s0047-259x(03)00096-4

[94] K. Pearson, “VII. Note on regression and inheritance in the case of two parents,” *Proceedings of the Royal Society of London*, vol. 58, no. 347–352, pp. 240–242, Dec. 1895, doi: 10.1098/rspl.1895.0041

[95] S. M. Smith et al., “Network modelling methods for FMRI,” *NeuroImage*, vol. 54, no. 2, pp. 875–891, Jan. 2011, doi: 10.1016/j.neuroimage.2010.08.063

[96] G. Varoquaux, F. Baronnet, A. Kleinschmidt, P. Fillard, and B. Thirion, “Detection of Brain Functional-Connectivity difference in post-stroke patients using Group-Level covariance modeling,” in *Springer eBooks*, 2010, pp. 200–208. doi: 10.1007/978-3-642-15705-9_25

[97] I. Steinwart and A. Christmann, *Support vector machines*. Springer Science & Business Media, 2008

[98] D. R. Cox, *Principles of statistical inference*. Cambridge University Press, 2006

[99] C. Cortes and V. Vapnik, “Support-vector networks,” *Machine Learning*, vol. 20, no. 3, pp. 273–297, Sep. 1995, doi: 10.1007/bf00994018

[100] A. E. Hoerl, A. E. Hoerl, and C. Hoerl, “Application of ridge analysis to regression problems,” *Chemical Engineering Progress*, Jan. 1962, [Online]. Available: http://www.scienceopen.com/document/vid/77767d4d-bc39-4026-856b-9fdf2075fddb

[101] S. R. Safavian and D. A. Landgrebe, “A survey of decision tree classifier methodology,” *IEEE Transactions on Systems*, Man, and Cybernetics, vol. 21, no. 3, pp. 660–674, Jan. 1991, doi: 10.1109/21.97458

[102] L. Breiman, “Random forests,” Machine Learning, 45(1):5–32, 2001

[103] M. Schonlau and R. Y. Zou, “The random forest algorithm for statistical learning,” *Stata Journal*, vol. 20, no. 1, pp. 3–29, Mar. 2020, doi: 10.1177/1536867x20909688

[104] T. K. Ho, “Random decision forests,” *Machine Learning*, Nov. 2002, doi: 10.1109/icdar.1995.598994

[105] T. Hastie, R. Tibshirani, and J. H. Friedman, *The elements of statistical learning*. 2001. doi: 10.1007/978-0-387-21606-5

[106] A. Y. Ng and M. I. Jordan, “On Discriminative vs. Generative Classifiers: A comparison of logistic regression and naive Bayes,” *Neural Information*

Processing Systems, vol. 14, pp. 841–848, Jan. 2001, [Online]. Available: http://papers.nips.cc/paper/2020-on-discriminative-vs-generative-classifiers-a-comparison-of-logistic-regression-and-naive-bayes.pdf

[107] G. H. John and P. Langley, "Estimating continuous distributions in Bayesian classifiers," *Uncertainty in Artificial Intelligence*, pp. 338–345, Aug. 1995, [Online]. Available: https://dblp.uni-trier.de/db/conf/uai/uai1995.html#JohnL95

[108] S. Hochreiter and J. Schmidhuber, "Long Short-Term memory," *Neural Computation*, vol. 9, no. 8, pp. 1735–1780, Nov. 1997, doi: 10.1162/neco.1997.9.8.1735

[109] M. Schuster and K. K. Paliwal, "Bidirectional recurrent neural networks," *IEEE Transactions on Signal Processing*, vol. 45, no. 11, pp. 2673–2681, Jan. 1997, doi: 10.1109/78.650093

[110] Z. C. Lipton, J. Berkowitz, and C. Elkan, "A Critical Review of Recurrent Neural Networks for Sequence Learning," *arXiv*, May 2015

[111] R. Pascanu, T. Mikolov, and Y. Bengio, "On the difficulty of training recurrent neural networks," *International Conference on Machine Learning*, pp. 1310–1318, Jun. 2013, [Online]. Available: http://proceedings.mlr.press/v28/pascanu13.pdf

[112] A. Sherstinsky, "Fundamentals of Recurrent Neural Network (RNN) and Long Short-Term Memory (LSTM) network," *Physica D: Nonlinear Phenomena*, vol. 404, p. 132306, Mar. 2020, doi: 10.1016/j.physd.2019.132306

[113] Y. Gal and Z. Ghahramani, "A theoretically grounded application of dropout in recurrent neural networks," *Neural Information Processing Systems*, vol. 29, pp. 1027–1035, Dec. 2016, [Online]. Available: https://papers.nips.cc/paper/6241-a-theoretically-grounded-application-of-dropout-in-recurrent-neural-networks.pdf

[114] M. Mokhtari, B. Abdulrazak, and H. Aloulou, *Smart homes and health telematics, designing a better future: urban assisted living: 16th International Conference, ICOST 2018, Singapore*, Singapore, July 10-12, 2018, Proceedings. Springer, 2018.

[115] R. Kohavi, "A study of cross-validation and bootstrap for accuracy estimation and model selection," *International Joint Conference on Artificial Intelligence*, vol. 2, pp. 1137–1143, Aug. 1995, [Online]. Available: http://ijcai.org/Proceedings/95-2/Papers/016.pdf

[116] P. J. Uhlhaas and W. Singer, “Neural synchrony in Brain Disorders: Relevance for Cognitive Dysfunctions and Pathophysiology,” *Neuron*, vol. 52, no. 1, pp. 155–168, Oct. 2006, doi: 10.1016/j.neuron.2006.09.020

[117] T. Eslami, V. Mirjalili, A. C. M. Fong, A. R. Laird, and F. Saeed, “ASD-DiagNet: A hybrid learning approach for detection of autism Spectrum disorder using FMRI data,” *Frontiers in Neuroinformatics*, vol. 13, Nov. 2019, doi: 10.3389/fninf.2019.00070

[118] S. Mostafa, L. Tang, and F.-X. Wu, “Diagnosis of autism spectrum disorder based on eigenvalues of brain networks,” *IEEE Access*, vol. 7, pp. 128474–128486, Jan. 2019, doi: 10.1109/access.2019.2940198

[119] S. Parisot et al., “Spectral Graph convolutions for Population-Based Disease Prediction,” in *Lecture Notes in Computer Science*, 2017, pp. 177–185. doi: 10.1007/978-3-319-66179-7_21

[120] X. Yang, M. Islam, and A. M. A. Khaled, “Functional connectivity magnetic resonance imaging classification of autism spectrum disorder using the multisite ABIDE dataset,” *IEEE Access*, May 2019, doi: 10.1109/bhi.2019.8834653.